Effect of Surface Stress on Micromechanical Cantilevers for Sensing Applications

by

Monrudee Liangruksa

Thesis submitted to the faculty of
Virginia Polytechnic Institute and State University
in partial fulfillment of the requirements for the degree of

Master of Science
in
Engineering Mechanics

Surot Thangjitham, Chair
Scott W. Case
Mark S. Cramer

July, 3 2008
Blacksburg, Virginia

Keywords: Microcantilever, surface stress, Lennard-Jones potential, atomic force, sensor.

Effect of Surface Stress on Micromechanical Cantilevers for Sensing Applications

by

Monrudee Liangruksa

ABSTRACT

Three models for surface stress loading effect on a micromechanical cantilever are proposed as concentrated moment acting at the free end (Model I), concentrated moment plus axial force acting at the free end (Model II), and uniformly distributed surface force acting along the microcantilever (Model III). Solution to Model I loading is based on the Stoney formula, assuming that the microcantilever is subjected to pure bending and deformed with a constant curvature. Model II takes into account the clamping effect in such a way that an additional axial force is introduced. The deflections resulting from Models I and II surface stress loading effect are solved by Euler-Bernoulli beam theory. In Model III, the effect of surface stress is modeled as uniformly distributed surface force that causes both uniformly distributed bending moment and axial force acting along the axis of the microcantilever. The energy method is then used to obtain the governing equation and boundary conditions for Model III displacement. Comparison of the results obtained by the three models with those by the finite element method and experi-

ment indicates that Model III is the most realistic model for surface stress loading effect to obtain the deflection of a microcantilever.

Model III for surface stress loading effect is then used to demonstrate the applications of a microcantilever in sensor technology through the measurement of tip deflection under an atomic adsorption as the source of surface stress. Dual attractive or repulsive characteristics of interactions between a pair of mercury atoms are described in terms of Lennard-Jones potential. The force per unit atomic spacing induced by the adjacent free surface atoms of a monolayer is then computed using the potential. The sensitivities of atomic spacing and monolayer thickness to the tip-deflection of a microcantilever are studied in this research.

ACKNOWLEDGMENTS

This thesis could not have been written without Dr. Surot Thangjitham who not only served as my advisor but also taught, encouraged, and assisted me throughout my master program. His kindness, insightful guidance, and patience are deeply admired. It has been my honor to be his student. Additionally, I also would like to thank Dr. Scott Case and Dr. Mark Cramer for serving as my committee members and providing some valuable advice.

I am also greatly indebted to all of my teachers in the past from Silpakorn University for the valuable knowledge in physics and from Virginia Tech for the priceless engineering education. It's not only the academic knowledge which I have learned from them, but also the wonderful thoughts about life.

Additionally, special thanks go to all Thai friends at Virginia Tech. They have always encouraged and supported me. This is such a nice community which I never expected to see, but Thai students at Virginia Tech have shown me their spirits, warmth, and friendships. There are so many people that I couldn't list all their names in just a piece of paper. Also, I would like to express my special thanks to my officemates. Their valuable discussions and supports throughout the years are greatly appreciated.

Most importantly, I would like to express my deepest thanks and appreciation to my parents. Their endless loves, encouragements, and prayers for me have kept

me strong to achieve my goals. Also, thanks go to every people in my family who are always beside me and supporting me.

Last but not least, I am grateful to the Royal Thai Government for providing me with the scholarship so I can pursue my dream to become the best I can be. I am very proud and it is also my great honor to be selected by the Thai Government as one of the recipients to receive the opportunity to study abroad.

CONTENTS

LIST OF TABLES

LIST OF FIGURES

CHAPTER 1

Introduction

Microelectromechanical systems (MEMS) and nanoelectromechanical systems (NEMS) have played a role in sensor technology based on the transduction principle [1]. Functionalities of NEMS and MEMS are based on mechanical motion of their components, but NEMS are smaller and hold promise to improve capabilities of ultra sensitive detection at the molecular scale. A micromechanical cantilever (microcantilever) is usually made of Si, SiN or polymer. It is similar to a probe used in atomic force microscope (AFM) found generally in the field of MEMS and NEMS. Operation of MEMS and NEMS' sensors involve measurements of deflections, resonant frequency or damping characteristics of the microcantilever. The mode of sensor operation could be either static or dynamic depending on the measured parameter. In the static mode, deformations of microcantilevers are caused by stresses generated on their surfaces. Moreover, they do not exhibit functional movements if there is not a change in the input stimulus. In the dynamic mode, the resonant frequency of microcantilever sensors depends on the attached mass as well as viscoelastic properties of medium and the resonant frequency of the microcantilever with analyte molecules is lower than that of no analyte molecules.

Micro and Nanoelectromechanical systems (MEMS and NEMS) can be used as physical, chemical or biological sensors since molecular binding, chemical reaction, and specific biomolecular interactions can affect mechanical characteristics of

the microcantilevers. This idea has been brought to sensor technology based on the mechanical response of micro-fabricated cantilevers as used in scanning force microscopy. Scaling down the dimension of a microcantilever to a nanocantilever helps to improve their ultra sensitive detections in sensing applications. Without external magnetic, gravitational, and electrostatic forces, mechanical responses of microcantilevers in MEMS and NEMS are caused by a gradient of mechanical stress produced in the device. The stress can be generated by changes in temperature in the case of microcantilevers made of two layered materials with different coefficients of thermal expansion. However, molecular adsorption and interfacial chemical reactions may also produce significant surface stress changes on the microcantilevers. Long before the first micro-fabricated cantilever has been produced, the study of surface stress changes had been limited. With availabilities of mass production of AFM probes and the optical lever readout, real-time changes of surface stress are easier to measure.

A microcantilever designed for chemical sensing usually has its surface modified with a deposited receptor layer. This layer must be thin and uniform to avoid changes in mechanical properties and to generate a uniform stress. However, the exact mechanism to explain origins of the surface stress is not completely understood. Basically, the microcantilever deflection can be explained in terms of energy transfer between surface free energy and elastic energy associated with structural bending of the microcantilevers [2]. The surface stress and substrate curvature are generally determined by Stoney's formula making a linear analysis of small

deflection. The Stoney model explains the result of differential surface stress as a concentrated moment applied at the free end of the microcantilever and assumes a uniform curvature for the whole deflected structure, but it always overestimates the deflections.

1.1 The Study of Surface Stress Effects to the Static Mode of Sensors

In this study, three models of surface stress effects to the static mode of sensors on a micromechanical cantilever are investigated. The first model is based on the Stoney model describing the differential surface stress as a concentrated moment applied at the free end of the microcantilever (Model I). The next model is different from the Stoney model in such a way that it takes into account the clamping effect as the axial load component at the microcantilever's end (Model II). The surface stress effects in the third model are considered as uniformly distributed forces on the upper surface of the microcantilever [3]. These forces cause bending moment per unit length and uniform distributed axial stresses along the microcantilever (Model III).

The Euler-Bernoulli beam theory is introduced to calculate the results of surface stress effects as deflections of the first two models. Whereas the governing equation of the third model is obtained by energy method and then its numerical solution is compared with the finite element method. The surface stress effects of the proposed three models under different loading scenarios are then evaluated. Though origins of the surface stress are not completely understood, they are generally described as a result of induced stresses within surface atoms that is when

surface atoms attract to each other, this tend to curve the surface resulting in a concave surface curvature. If surface atoms repel each other, this gives a result in a convex surface curvature. Surface stress is then simulated as these atomistic interactions between surface atoms.

In the present work, the adsorption of a monolayer of mercury on the microcantilever is considered; the Lennard-Jones potential is then employed to describe the dual attractive or repulsive interactions between a pair of mercury atoms. The energy potential is assumed that the first atomic layer on the microcantilever surface plays a dominant role in the microcantilever's deflections. Mercury atoms in the attached film are attracted and repulsed according to the Lennard-Jones potential formula. Forces per atomic width spacing of a mercury monolayer can be determined by the input data of the Lennard-Jones constants, atomic spacing of the atoms, and thickness of the monolayer. Based on three models of surface stress effects, these forces induced in the surface atoms could then be substituted in the governing equations of the three models. The deflection's results are compared with the experimental data done by Dareing et al. [2].

The physical property of the adsorbates can be defined by the attractive and repulsive constants in the Lennard-Jones potential. Therefore, these two parameters would affect the microcantilever deflections. The model of surface stress effects as uniformly distributed forces on the microcantilever surface is used to investigate the effect of these constants since the deflection results by this model compares favorably with the experimental result. Also, this model will be employed to study

the effects of the atomic spacing and the thickness of atomic monolayer of the coating.

1.2 Objectives of the Thesis

A general idea behind the physical, chemical or biological sensors is that atomic adsorption onto microcantilevers produces surface stress changes or mass loading effects which bring to the bending or vibration of microcantilevers, respectively. In this thesis the bending mode or static mode of a sensor is studied. The three objectives are as follows::

- Study the sources of surface stress and model their effects on a microcantilever in sensing applications. In addition, film stress and substrate curvature are investigated.

- Obtain the governing equations for models of surface stress effects and introduce numerical data to obtain the resulting deflections.

- Apply the model to the problem of a mercury monolayer on the surface and study effects of atomic spacing and the monolayer's thickness of mercury atoms to the bending.

CHAPTER 2

Literature Review

In 1959, Richard Feynman gave a very famous talk called "There's a Plenty Room at the Bottom" [4] and 23 years later he gave a talk entitled "Infinitesimal Machinery" [5]. These two talks helped give birth to the new field of nanotechnology. It is constantly evolving as commercial and academic interest. The important development turning nanotechnology into this broad field today is Scanning Tunneling Microscope (STM) invented by Binnig [6]. Quickly it was followed by the development of a whole family of related techniques. All of these techniques are operated by measuring a local property, such as height, optical absorption, or magnetism, with a probe or tip placed very close to the sample. The most important technique is Atomic Force Microscopy (AFM) [7]. These techniques opened up many new areas of science and engineering at the atomic and molecular level.

Atomic Force Microscopy (AFM) has proven to be an excellent tool for imaging a wide class of systems such as semiconductors, minerals, polymers, and biomaterials. Forces are measured by monitoring the deflection of a flexible cantilever in the AFM. Today, mass production of well defined cantilevers in AFM with dimensions on the order of microscale and nanoscale can be obtained by micro and nanomachining techniques. Moreover, microcantilevers are the most structures found generally in the field of microelectromechanical systems (MEMS). Typically, they are fabricated from Si, SiN or polymers. However, these materials have low

reflectivities which make them a poor choice for optical beam deflection. Though metal such as gold or aluminum has been introduced to coat on cantilevers made from silicon or silicon nitride to increase the reflectivity, this can produce the temperature sensitivity giving a significant error. This problem can be avoided by adding a metallic reflector pad to the cantilever end instead the metallic layer [8].

Microcantilevers are the excellent tools with high sensitivity in a number of innovative sensing applications. Many research groups are trying to develop micro and nanocantilever arrays as sensing applications [9] such as humidity sensors, herbicide sensors [10], temperature sensors [11], viscosity sensors [12], etc. [13-16]. In addition to a number of innovative chemical and biological sensors have emerged, the devices with simple design microcantilever are very attractive as transducers for these sensors. Chemical reactions, molecular binding, and specific biomolecular [14, 17-18], have been detected by the static deflection of microfabricated cantilever beam [8] which are usually used in Scanning Force Microscopy.

Micro and nanocantilever sensors have many advantages over the competing technologies in terms of the high sensitivity, easy mass production, low cost, simple procedure, low analyte requirement and quick response. In biological applications, the sensor translates biomolecular recognition into bending of the microcantilever [17]. Surface stress is induced by intermolecular forces from the adsorption of analyte molecules onto the microcantilever resulting in bending of the microcantilever. The surface stress induced during the formation of self-assembled monolayer is presented by Godin et al. [19]. The goal of this kind of measurements is gaining

some insight into the origins of the induced stresses and inter-molecular forces involved during the formation of these self-assembled structures. In the size domain of microelectromechanical system (MEMS), surface to volume ratio increases as microstructure scale decreases. Owing to this reason, surface stresses can be overwhelming and very important in microstructures.

The basic principle of these microcantilever sensors is based on the measurement of the nanometer-scale variation of the static mode and dynamic mode of the microcantilever owing to molecular adsorption on its surface [20]. The dynamic mode [13, 21] detects the resonant frequency shift driven by surface stress. The higher sensitivity of a cantilever is improved by scaling down to micro and nanoscale. Decreasing cantilever dimension gives much higher resonant frequencies than larger one, while providing the same spring constants. Therefore it is possible to detect smaller forces since smaller cantilevers have lower coefficient of viscous damping [22]. This can detect even very small amounts of molecular interactions. The static mode is commonly used to perform the measurements in liquids because the quality factor of cantilevers in liquids is low, decreasing the sensitivity of the dynamic mode. The mechanism of static mode (microcantilever bending) is to measure the differential surface stress when molecular adsorption preferentially occurs on one side of the microcantilever more than the other side. The difference of surface stress between surfaces is relaxed by unequal expansion or contraction of both surfaces which results in a microcantilever bending [23, 24].

The surface stress, which is a mechanical property of solid surfaces, arises when surface atoms or thin films undergo some dynamic micro-structural process resulting in a change in density while being rigidly bound to its substrate. It is defined as the force per length which has to be applied when a surface is extended or compressed. If bond strengths between surface atoms are stronger than that of surface atoms and sub-surface atoms, the attractive forces between these surface atoms would tend to curve the surface towards the surface resulting in a tensile surface stress. But, if surface atoms repel each other, a compressive surface stress is induced which causes a convex surface structure. The sources of surface stress can be the surface reconstruction [25], interactions between a surface and adsorbates [26-29] or the expansion of a deposited thin film arising from temperature changes. It plays a role in surface reconstruction [30], shape transitions in nanoscale particles, surface diffusion, epitaxial growth, and self-assembled domain patterns. The origins of compressive or tensile surface stresses are generally described as molecular or atomic adsorption on surfaces. Surface stresses will be compressive or tensile depending on adsorbate-surface interactions. Also, elastic energy associated with structural bending of the cantilevers and energy transfer between surfaced free energy is used to explain deflections of microcantilevers [31]. The surface stress relating to the energy change is produced when a surface is elastically stretched to the resulting strain. In clean surfaces, the surface stress arises from the interactions between neighboring surface atoms and of those with the environment. In the bulk, atoms are positively charged and bound by sharing either localized

or delocalized electrons. At the surface, electrons react to the missing atoms and bounded charge. Thus, the electronic charge is redistributed, flowing into the space between the surface atoms. The surface stress has been modified since adsorption of molecules on the surface produces a charge distribution between the surface and the adsorbates. In addition to the charge transfer mechanism, the lateral interaction between adsorbed molecules plays an important role in the adsorption driven surface stress.

Changes of the surface stress drive the microcantilever to bend. The surface stress is often computed by Stoney equation [32] with a uniform curvature as following:

$$\frac{1}{R} = \frac{6\,(1-\nu)}{E h_s^2}\Delta\sigma \tag{2.1}$$

where R is the radius of curvature, E is the Young's modulus, ν is Poisson ratio, h_s is the thickness of the cantilever, and $\Delta\sigma$ is the difference in surface stress between the top and the bottom of the microcantilever. Surface stress has been studied extensively and Stoney formula is a cornerstone for curvature based analysis. In 1909, Stoney found that a protective layer of copper electrodeposited on silver films easily peeled off when the thickness of the copper layer was in excess of 10 μm [32, 33]. He observed a metal film deposited on a thick substrate being in a state of tension or compression which can consequently strain the substrate to bend when no external loads apply.

The key features of the Stoney equation are a uniform curvature for the whole deflected structure and the use of a linear analysis of small deflections. It is based

on many assumptions [33] which are: *(i)* both film and substrate thicknesses are small compared to the lateral dimensions; *(ii)* the film thickness is much less than the substrate thickness; *(iii)* both the substrate material and the film material are isotropic, homogenous and linearly elastic; *(iv)* edge effects near the periphery of the substrate are inconsequential and all physical quantities are invariant under change in position parallel to the interface; (v) all stress components in the thickness direction vanish throughout the material; and *(vi)* the strains and rotations are very small. As a result, the Stoney formula does not agree well with the experiment data [33, 34] for structures under large deflection of thick film. Using linear analysis, Klein [32] and Freund et al. [31] conclude that Stoney formula holds for the structure with a large ratio of substrate thickness to film/coating thickness, i.e. "thin" film case.

Another characteristic of Stoney formula is to model the surface stress as a moment applied at the structure's free end. Freund et al. [33] still use uniform curvature as the kinetic assumption and the problem of uniform curvature is solved by the principle of minimum potential energy. As the influence of thin film stress through system curvature measurements are based on the assumption of uniform curvature over the entire film/substrate system [35], the accuracy of the approximation deteriorates when the level of curvature nonuniformity increases. Feng et al. [36] presented methods for the film/substrate system subjecting to nonuniform misfit strain and temperature changes. This film stresses are found to depend on system curvature nonlocally by using perturbation analysis. The methods can be

extended to nonuniform substrate thickness for the film/substrate with any nonuniform misfit strain. Sader [37] studied about surface stress induced deflections of cantilever V-shaped plates and concluded that a differential surface stress on the plate is equivalent to the loading of the free edges by the corresponding moment per unit length. Godin et al. [38] introduced a method to compute the surface stress from the cantilever deflection by using readily measurable cantilever properties, such as its geometry, spring constant, and Poisson's ratio. In addition, Miyatani and Fujihira [39] investigated the bending of commercial rectangular cantilevers under the concentrated load mode and the bending moment mode.

Dareing et al. [2] propose a model for adsorption-induced surface stress based on atomic or molecular interaction explaining the mechanism of bending in terms of atomic energy and elastic energy. The model gives insight into the interatomic forces that play a role in creating adsorption-induced surface stress and resultant of mechanical bending of microcantilevers. Minimizing the total potential function which derives from the Lennard-Jones potential and the elastic energy in the cantilever is used to determine the equilibrium configuration of the microcantilever. Mercury adsorption on gold-coated microcantilevers was tested by experiment and compared with simulation model.

Analytical models predicting the deflection and force of a biomaterial cantilever considering the clamping effect are presented by Ramos et al. [40]. The models are based on a silicon microcantilever with a thin gold film on one side undergoing measurable bending corresponding to bimetallic effect. The Stoney model derived

from a moment applied at the free end of the cantilever and the axial load model taking into account the clamping effect are studied. In this case, the differential stress in the microcantilever is created due to unequal thermal expansion coefficients of the silicon substrate and the gold coating. This infinitesimal heat change which can be detected by the biomaterial microcantilevers is in the range of femtojoules. The effect of surface stress on the resonant frequency of microcantilevers was predicted by a model of McFarland [41]. Since surface stress tends to stretch or compress the beam, the resonant frequency for any given bending mode will either decrease or increase. With this model, one can compute the surface stress which acts on microcantilevers by measuring resonant frequencies.

There are many group researches interested in the static mode of microcantilever sensors. For example, Zhang et al. proposed three models of surface stresses on rectangular beam [41]. The surface stresses are modeled as a corresponding concentrated moment at the free-end, a corresponding concentrated moment plus a corresponding concentrated axial load at the free-end, and a corresponding uniformly distributed axial stress plus bending moment per unit length along the beam. The last model of surface stress can explain the local stressors caused by behavior of the thin layer on the substrate [42]. Zhang et al. [3] use Euler-Bernoulli beam model to analyze the small deflection due to the surface stresses and also studied about the stiffening effect of tensile surface stress. They found that modeling the surface stress as a corresponding concentrated moment at the free-end overestimates the deflection, because this ignores the stiffening effect of the tensile

stress. Since scaling-down of the macro devices might increase the nonlinearity, it is challenging to find out how much one could decrease the dimension of a device and still uses the linear form of differential equation for modeling the system. The difference of linear and nonlinear analysis of a baseline microcantilever which represents the fundamental element of a microstructure is theoretically investigated by Changizi [43].

CHAPTER 3

Mechanics of Thin Films and Effects of Surface Stress

A thin film is a thin layer ranging from fractions of a single layer of atoms to several micrometers in thickness. They have been used in engineering systems and have been adapted to a wide variety of functions as following [44]:

- Thin film technology has been used in highly integrated electronic circuits in such a way that confinement of electric charge relies largely on interfaces between materials with different electronic properties.

- Another thin film technology is coating the surface for structural material protection at high temperature. For example, in gas turbine engine, thin films are employed to increase engine efficient and to significantly extend the lifetimes of the structures that they protect, because of their chemical inertness, stability at elevated temperatures and low thermal conductivity.

- The use of surface coatings prolongs the useful lifetimes of components subjected to friction and wear due to contact extended.

- Thin films are found to be integral parts of micro and nanoelectromechanical systems (MEMS and NEMS) which are designed to serve as sensors or actuators.

3.1 Overview of Thin Film

Thin films can be characterized into three types by its thickness comparing to the characteristic microstructural length scales such as the grain size, dislocation cell size, precipitate or particle spacing, etc. These three types are mechanically thin film, microstructurally thin film, and atomically thin film. In the case of mechanically thin film, the thin film either has no intrinsic structural length scales (amorphous film) or film thickness is much larger than the characteristic microstructural length scales. Generally, this kind of thin film has the thickness in the range of ten-hundred micrometers and is deposited on the substrate by plasma spray or physical vapor deposition, diffusion bonding, explosion cladding, or sintering. The continuum mechanics is a sufficient approach to analyze the stress of the film. In the second type of thin film, microstructurally thin film, the small dimension of the film is comparable to the characteristic microstructural size scale. This type of thin films is commonly found in microelectronic devices and magnetic storage media where the film thickness is greater than atomic or molecular dimensions. The mechanical properties of these films are strongly influenced by factors such as average grain size, grain shape, grain size distribution, grain to grain variations, and crystallographic texture. Thin films whose thicknesses are comparable to one or a few atomic layers are called atomically thin films. Examples include an adsorbed monolayer of gas or impurity atoms on a surface. The mechanical response of the atomically thin film tends to be more influenced by interatomic potentials and surface energy than by micromechanisms of deformation.

3.2 Sources of Film Stress

Fabrication is the important process to obtain the desirable thin film. However, this process typically results in internal stress in the film which can be in the magnitude sufficient to induce mechanical deformation, damage or failure. Knowledge about the sources and effects of stresses in thin film is necessarily employed in the fabrication processes to obtain a good thin film. During the fabrication, the intrinsic stress is developed by surface or interface stress, cluster coalescence reducing surface area, grain growth, impurities, phase transformations and structural damage due to the deposition process. The stress generally refers to the internal stress distribution in a material system with no applied traction at all external boundaries. When any thin film bonded to a substrate or any individual lamina within a multilayer material creates some state of residual stress over a size scale on the order of it thickness. If the film were relieved of the constraint of its neighboring layers, it would change its in-plane dimension and/or would become curved in the presence of the stress. If the internal distribution of mismatch strain is not compatible with a stress-free state, then some stress distributions will be left under these conditions.

After the fabrication of thin film, the stress called extrinsic stress arises from the physical effects such as temperature change with a difference in coefficients of thermal expansion between bonded elements, gravitational forces, composition segregation, chemical reactions and plastic deformation, etc.

3.3 Classification of Film Stress

Film stresses are usually classified into two categories. One category is growth stresses, which mean the presence of those stress distribution in films following growth on substrates or on adjacent layers. Growth stresses strongly depend on the film and substrate material, and on the substrate temperature during deposition, the growth flux, and growth chamber conditions. It's possible to follow the evolution of growth surface features and the corresponding evolution of average stress levels in the course of film formation because of advances in nonintrusive observational methods for in situ stress measurement and growth surface monitoring. These advances have provided new insights into the origins of film stress and have led to subdivision of the category of growth stresses into those stresses arising during various phases of the growth process and those which are present at the end of the growth process. Growth stresses are usually reproducible for a given process and the values at the end of growth remain at room temperature for a long time following growth processes. Growth stresses are also called intrinsic stresses. A second category of film stress arises from changes of stresses in physical environment of the film material following the fabrication process which is commonly called extrinsic stresses. In many cases, these stresses happen only when the film is bonded to a substrate.

Growth or intrinsic stresses for a particular material system, substrate temperature and growth flux depend on many factors. The most important among these factors probably is the bonding of the deposit to the substrate, the mobility

of atoms on the film material itself, and the mobility of grain boundaries formed during growth. Many mechanisms to explain stresses generation during film material deposition have been proposed. The most common among these have been reviewed by Doerner and Nix [45] as surface or interface stress, cluster coalescence reducing surface area, grain growth, impurities, phase transformations, and structural damage due to the deposition process. Extrinsic stresses are induced in films from external influences arising from the physical effects after the deposition process such as temperature change with a difference in coefficients of thermal expansion between bonded elements, piezoelectric response to an electric field, etc.

The stresses developed in thin films can lower the reliability of thin film electronic devices. An understanding of the origin of these stresses and the deformation controlling processes in thin films is needed in order to design these devices for improved mechanical reliability. The dimensions of the film would change if stresses in thin film were produced. The basic deformation mechanisms operating in bulk materials also apply to thin films and the constraint of the substrate is important in suppressing the operation of certain stress relaxation mechanisms, because the substrate is an important factor in the consideration of the film properties.

3.4 The Mechanics of Stresses in Thin Films on Substrates

It is essential to understand the origin of stresses in thin films on substrates [45]. Here a film which is totally free of stress is considered. Imagine removing it from the substrate and allow it to stand in a stress-free state as shown in Figure 3.1(a). Hence, the lateral dimensions of the film exactly match those of the substrate from

which it was removed in this state. It can always be reattached to the substrate without causing any stresses to be generated in either the film or substrate when the state of the film is not changed. If the dimensions of films change, elastic strains and stresses will develop when the film is reattached to the substrate. Then film is experienced a uniform volume change (dilational transformation strain,) in the detached state. This volume change or dilational strain is measured relative to that of the substrate. It is shown in Figure 3.1 (b) as a negative dilation (a volume shrinkage). The principle strain components are $\epsilon^T_{xx} = \epsilon^T_{yy} = \epsilon^T_{zz} = e^T/3$ in a pure dilational strain. There are many ways of the volume of a film might change relative to the substrate which is caused by different thermal expansion coefficients, structural or compositional changes in the film, annihilation of excess vacancies, dislocations, grain boundaries, and phase transformations.

To reattach the film to the substrate, a biaxial stress must be imposed on the film to elastically deform it so as to fitting the dimensions of the substrate again. This stress produces elastic strains ϵ^{el}_{xx} and ϵ^{el}_{yy} and that exactly balance these components of the transformation strain.

$$\epsilon^{el}_{xx} = \epsilon^{el}_{yy} = -e^T/3 \tag{3.1}$$

Using Hooke's law, this brings to a biaxial stress in the film.

$$\bar{\sigma} = \bar{\sigma}_{xx} = \bar{\sigma}_{yy} = \frac{E}{1-\nu}\epsilon^{el}_{yy} = -\frac{E}{1-\nu}\frac{e^T}{3} \tag{3.2}$$

From Figure 3.1(c), the tractions or forces applied at the edges of the film result in a pure biaxial stress state. Edge forces are removed after the film is again

perfectly bonded to the substrate. These tractions at the edges are removed by superimposing edge forces of opposite sign as shown in Figure 3.1(d). The additional forces remove the normal tractions from the edges of the film and produce shear stresses on the interface between film and substrate near the edges of the film. It is the shear stresses on the interface providing the forces to maintain the biaxial stress in the film. Hence these forces cause the substrate to bend elastically. The shear and normal stresses on the film/substrate interface are significant at very near the edges of the thin film with lateral dimensions much greater than the thickness of the film, because they can cause sliding and/or decohesion to occur. This might allow the biaxial stress in the film to be relaxed and can cause the film to peel off the substrate.

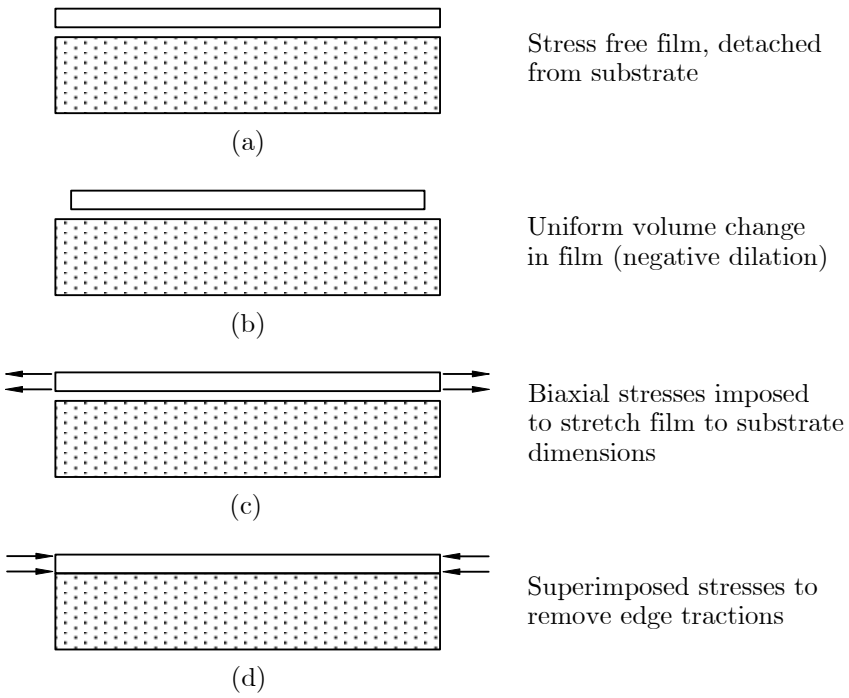

Figure 3.1: The development of film stress due to change in film volume.

3.5 Effects of Film Stress to Substrate Curvature and Stoney Formula

The presence of residual stress in films deposited on substrates and the effects of such stress on delamination and cracking were studied the early nineteenth century. For example, an antimony film deposited on a substrate was found to crack due to vibration or heat. Stoney found that copper electrodeposited as a protective layer on silver films easily peeled off when the thickness of the copper layer was in excess of 10 μm.

Stoney made the observations when no external loads were applied to the system of film and substrate, a metal film deposited on a thick substrate was in a state of either tension or compression and it would consequently strain the substrate to bend it. He introduced a simple analysis to relate the stress in the film to the amount of bending in the substrate. In his analysis, Stoney electrolytically deposited thin layers of nickel, 5.6 μm to 46.2 μm in thickness, on 0.31 mm thick steel rulers (substrate) which were 102 mm long and 12 mm wide. Stoney predicted from his analysis that the tensile stress in the nickel film exists in the range from 152 to 296 MPa for film thickness of 46.2 to 5.6 μm, respectively, by using measurements of the film thickness, the amount of bending of the steel ruler and the elastic modulus of steel.

Highly sophisticated experimental tools for measuring the curvature of substrates with deposited thin film have become available since Stoney's work. The concepts underlying his analysis have still been used for the estimation of film stresses in a wide variety of modern applications including microelectronics, opto-

electronics, and surface coatings in structural components. The Stoney formula for curvature and stress in a film-substrate system can be derived by using a number of different methods.

The Stoney formula is widely used in experimental work in which stress values are inferred from curvature measurement in thin films when they are bonded to the substrates. However, Stoney formula for a circular plate substrate is under these assumptions [44].

- According to the Kirchhoff hypothesis of circular thin plate theory, the substrates deform with the normal stress component $\bar{\sigma}_{zz} = 0$ everywhere, and material lines are straight and perpendicular to the mid-plane of the substrate prior to deformation and after deformation, so that $\epsilon_{rz} = \epsilon_{\theta z} = 0$.

- Since Stoney formula based on the system under small displacement, linear theory of elasticity is potentially applied to solve the problems.

- The material properties of the film do not have effects to the overall elastic stiffness of film-substrate system.

Also, assumptions of the formula concerning the deformation are:

- The deformation is axially symmetric, hence $\epsilon_{r\theta} = 0$.

- The curvature of the substrate mid-plane surface, is uniform.

- The in-plane strain of the mid-plane is a uniform, isotropic extension ϵ_0 and localized edge effects around the periphery of the film are ignored for the time being.

The formula can be obtained by a number of different approaches, for example, Stoney's method in 1909, energy method by Freund, and thin plate theory method by Schwarzer, etc. However, the advantage of using the energy method applied to the problem is able to handle complicated cases.

3.5.1 Stoney Method The amount of bending, as well as the thickness of the deposit, produce the tension on the interface between deposit and substrate. Stoney considered a layer of nickel of small thickness h_f deposited on a thin steel substrate of thickness h_s with Young's modulus E. As a result, the thin steel substrate is curved by the film of nickel to a radius causing bending moments for the steel. Let a be the depth from the surface of the substrate to the neutral axis.

$$\int_{h_s}^{0} \frac{E}{r}(a-x)\,x dx = 0, \qquad a = \frac{2}{3}h_s \tag{3.3}$$

If is the tension per unit area of section on the film of nickel

$$\bar{\sigma} h_f = \int_{h_s}^{0} \frac{E}{r}(a-x)\,dx = \frac{1}{6}\frac{E}{r}h_s^2 \tag{3.4}$$

The curvature can be determined by the deflections of the ruler (substrate) in a length l, as $r = l^2/(8z)$. Substituting the value of into above equation:

$$\bar{\sigma} = \frac{4}{3}\frac{E h_s^2 z}{h_f l^2} \tag{3.5}$$

This equation is true when the film of nickel is very thin. Since the properties of nickel closely resemble steel. It is easy to allow for the thickness of the nickel film on the assumption that the modulus of elasticity of nickel is the same as steel.

3.5.2 Freund's Method Suppose that a thin film is bonded to one surface of a substrate with uniform thickness h_s and assume that the substrate has the shape of a circular disk of radius R. The principal results of this section are independent of the actual shape of the outer boundary of the substrate. A cylindrical r-, θ-, and z-coordinate system is used with its origin at the center of the substrate midplane and with its z-axis perpendicular to the faces of the substrate, the midplane is at $z = 0$ and the film is bonded to the face at $z = h_s/2$. The substrate is so thin that $h_s << R$, and the film is very thin compared with the substrate. An elastic mismatch strain in thin film and the substrate is caused by thermal expansion effects, epitaxial mismatch, phase transformation, chemical reaction, moisture adsorption and/or other physical effect. The curvature of the substrate within the range of elastic response induced by the stress which is either an isotropic extension or compression in the plane of the interface could be estimated. The substrate is taken to be an isotropic elastic solid with elastic modulus, E_s, Poisson ratio, ν_s, and the elastic shear modulus, G_s, is related to the elastic modulus and Poisson ratio by $G_s = E_s/\left(2\left(1+\nu_s\right)\right)$.

In Figure 3.2, the substrate is initially separated from the film, stress-free and undeformed. The isotropic membrane force, σ, with dimensions of force/length, is maintained in the film. The magnitude of induces the elastic mismatch strain in the free film (may be either positive or negative). If a stress-free transformation strain of the film is not compatible with that of substrate material, the elastic mismatch strain and stress-free transformation strain are equal in magnitude but

opposite in sign. The strained film is then reattached to the substrate surface, after the external forces of maintaining the film tension is relaxed. It is in relaxation that the substrate becomes strained.

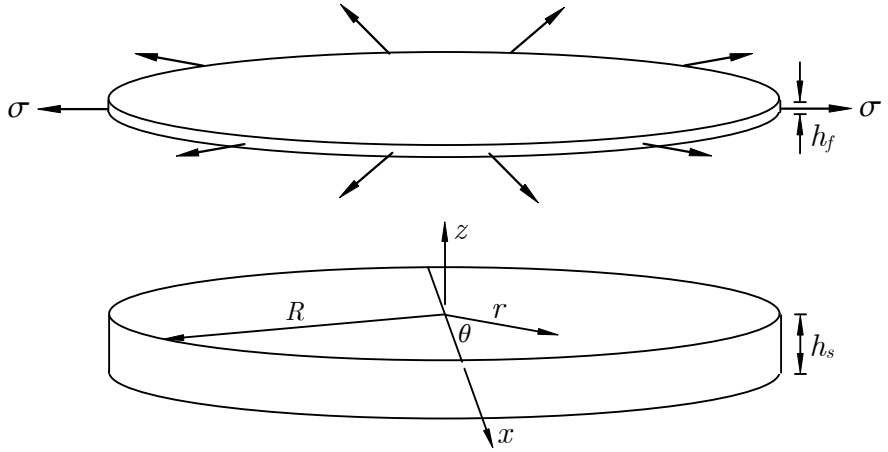

Figure 3.2: Distributed force σ acting on the film edge.

For the system features outlined above, the strain energy per unit volume at any point in the substrate material can be expressed in terms of the nonzero strain components as following:

$$U(r,z) = \frac{G_s}{1-\nu_s}\left(\epsilon_{rr}^2 + \epsilon_{\theta\theta}^2 + 2\nu_s\epsilon_{rr}\epsilon_{\theta\theta}\right) \tag{3.6}$$

where ν_s is the Poisson ratio and G_s is the elastic shear modulus.

With small deformation, the elastic strains appearing in Eq. (3.6) can be expressed in terms of the radial $u(r)$ and out-of-plane $w(r)$ displacement components of a point $(r,0)$ on the substrate midplane, as

$$\epsilon_{rr}(r,z) = u'(r) - zw''(r), \qquad \epsilon_{\theta\theta}(r,z) = \frac{1}{r}u(r) - \frac{z}{r}w'(r) \tag{3.7}$$

where the prime represents differentiation with respect to the argument.

The principle of stationary potential energy is introduced to determine optimal values of plausible parametric forms for $u(r)$ and $w(r)$ to minimize potential energy. For small deflections, the radial deformation and the transverse deformation are uncoupled and the choice of midplane displacement is

$$u(r) = \epsilon_0 r, \qquad w(r) = \frac{1}{2}\kappa r^2 \tag{3.8}$$

where κ represents the inverse of radius of curvature, of this plane. This is a reasonable choice of midplane displacement in the absence of the edge effects, because points on the substrate midplane are the same and therefore the curvature should be uniform over the midplane. The in-plane normal strain is $\epsilon_{\theta\theta} = \epsilon_{rr} = \epsilon_0 - \kappa z$ where ϵ_0 is the extensional strain of the substrate midplane and κz represents the extensional strain due to the bending at any position z with respect to the midplane to the substrate. The resistance to the deformation can be expressed in terms of the biaxial elastic modulus of the substrate material, $\bar{E}_s$, as the state of deformation is equi-biaxial strain at each point of the substrate. The ratio of equi-biaxial stress to equi-biaxial strain is the biaxial elastic modulus in an isotropic material. It depends on the elastic modulus E_s and Poisson's ratio ν_s. The extensional strain ϵ_{rr} is given by

$$\epsilon_{rr} = \frac{1-\nu_s}{E_s}\bar{\sigma}_{rr} = \frac{1}{\bar{E}_s}\bar{\sigma}_{rr} \tag{3.9}$$

where $\bar{E}_s = E_s/(1-\nu_s)$ is the biaxial modulus of the substrate.

The strain energy density in the substrate is expressed by $U(r,z) = \bar{E}_s(\epsilon_0 - \kappa z)^2$.

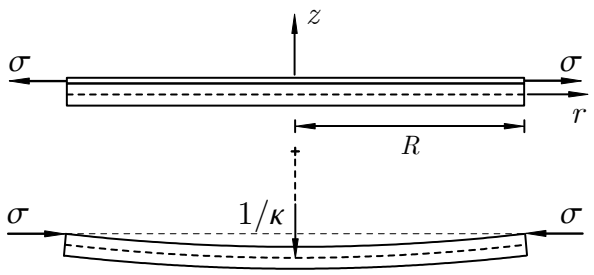

Figure 3.3: Curvature due to strain mismatch in film-substrate system.

The total potential energy of deformed state in the substrate can be written as

$$\begin{aligned}\Pi(\epsilon_0,\kappa) &= 2\pi\int_0^R\int_{-\frac{h_s}{2}}^{\frac{h_s}{2}} U(r,z)\,r dr dz + 2\pi\sigma u_r\left(R,\frac{h_s}{2}\right)R \\ &= \pi R^2\bar{E}_s h_s\left(\epsilon_0^2+\frac{1}{12}\kappa^2 h_s^2\right)+2\pi R^2\sigma\left(\epsilon_0-\frac{1}{2}\kappa h_s\right) \qquad (3.10)\end{aligned}$$

Minimize the total potential energy Π with respect to variations in its arguments requiring that $\partial\Pi/\partial\epsilon_0 = 0$ and $\partial\Pi/\partial\kappa = 0$. Hence $\epsilon_0$and κ are obtained as

$$\epsilon_0 = -\frac{\sigma}{\bar{E}_s h_s} \qquad (3.11)$$

and

$$\kappa = \frac{6\sigma}{\bar{E}_s h_s^2} \qquad (3.12)$$

The sign of curvature, κ, and membrane stress σ are the same. The substrate becomes convex when a tensile mismatch stress is applied on the face of the thin film and substrate. Let h_f be the thickness of the film, then the mean stress $\bar{\sigma}_m$ in the film is given by

$$\bar{\sigma}_m = \frac{\sigma}{h_f} \qquad (3.13)$$

Equation (3.12) is the Stoney formula which relates curvature and stress in

thin film which does not involve the properties of the film material. The stress in a thin film by Stoney formula is described by the stress in a thin film deposited on a rectangular substrate based on uniaxial state of stress. Hence, the substrate biaxial modulus $\bar{E}_s$ did not involve in his expression. From Eq. (3.13), the elastic mismatch strain ϵ_m corresponding to the stress $\bar{\sigma}_m$ is

$$\epsilon_m = \frac{\sigma}{\bar{E}_s h_f} \tag{3.14}$$

where $\bar{E}_s$ is the biaxial elastic modulus of the film material and h_f is the film thickness.

The location ($z = a$) of the unstrained neutral plane can be determined from Eqs. (3.7), (3.8), (3.11) and (3.12) under the condition $\epsilon_{rr}(r, a) = 0$.

$$a = \frac{\epsilon_0}{\kappa} = -\frac{1}{6} h_s \tag{3.15}$$

Hence, the neutral plane always lies at a distance $h_s/6$ from the midplane of the substrate with the opposite direction away from the film as shown in Figure 3.4. With the approximation of Stoney formula, it implies that the difference among the curvatures of the midplane, neutral plane, top face, and bottom face of the substrate are negligibly small.

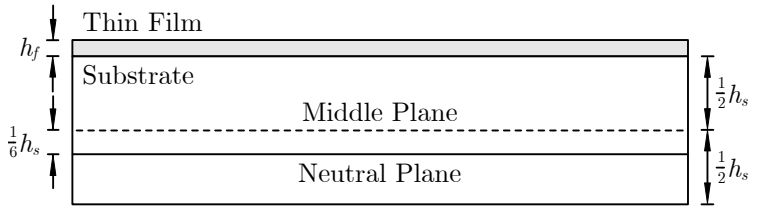

Figure 3.4: The location of the neutral plane in the substrate.

3.5.3 Plate Theory Method A thin plate is a plate whose thickness is small compared with the dimensions in the other two directions. When a plate is subjected to bending, it is stretched at some points and compressed at others. The plane on which no extension or compression occurs is referred to as the neutral plane or neutral surface. It is typically lies at the half of plate's thickness when no external forces apply [46].

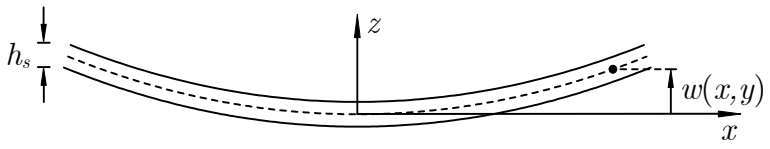

Figure 3.5: Bending of a plate.

Figure 3.5 shows the origin of the coordinate system on the neutral surface and z-axis perpendicular to the plate's surface. The xy-plane is the undeformed and denotes the vertical displacement of a point on the neutral surface in the z direction. The displacement components for points on the neutral surface is given by

$$u_x^{(0)} = u_y^{(0)} = 0, \qquad u_z^{(0)} = w(x, y) \tag{3.16}$$

where $u_x^{(0)}$, $u_y^{(0)}$, and $u_z^{(0)}$are displacement components at point (x, y) on the neutral surface in the x, y, and z-directions, respectively.

Considering the thin plate with only slightly bent, the approximation of $\bar{\sigma}_{xz} = \bar{\sigma}_{yz} = \bar{\sigma}_{zz}$ on both surfaces of the plate are small within the thin plate compared with the remaining components of the stress tensor everywhere in the plate. This condition is used to determine the components of the strain tensor. The stress

tensor can be written in terms of the strain tensor by

$$\bar{\sigma}_{ij} = \frac{E}{1+\nu}\left(\epsilon_{ij} + \frac{\nu}{1-2\nu}\delta_{ij}\epsilon_{kk}\right) \tag{3.17}$$

where $\bar{\sigma}_{ij}$ is the stress tensor, ϵ_{ij} is the strain tensor, E is the Young's modulus and ν is the Poisson's ratio.

$$\bar{\epsilon}_{ij} = \frac{1}{E}\left((1+\nu)\,\sigma_{ij} - \nu\delta_{ij}\bar{\sigma}_{kk}\right) \tag{3.18}$$

Since the plate is very thin, the stresses $\bar{\sigma}_{xz}$, $\bar{\sigma}_{yz}$, and $\bar{\sigma}_{zz}$ are approximately zero, hence

$$\bar{\sigma}_{xz} = \frac{E}{1+\nu}\epsilon_{xz}, \qquad \bar{\sigma}_{yz} = \frac{E}{1+\nu}\epsilon_{yz} \tag{3.19}$$

$$\bar{\sigma}_{zz} = \frac{E}{(1+\nu)\,(1-2\nu)}\left[(1-\nu)\,\epsilon_{zz} + \nu\,(\epsilon_{xx}+\epsilon_{yy})\right] \tag{3.20}$$

Since stress in z-direction is zero,

$$\frac{\partial u_x}{\partial z} = -\frac{\partial u_z}{\partial x}, \qquad \frac{\partial u_y}{\partial z} = -\frac{\partial u_z}{\partial y}, \qquad \epsilon_{zz} = -\frac{\nu}{1-\nu}\,(\epsilon_{xx}+\epsilon_{yy}) \tag{3.21}$$

But u_z can be written as $w(x,y)$

$$\frac{\partial u_x}{\partial z} = -\frac{\partial w}{\partial x}, \qquad \frac{\partial u_y}{\partial z} = -\frac{\partial w}{\partial y} \tag{3.22}$$

$$u_x = -z\frac{\partial w}{\partial x}, \qquad u_y = -z\frac{\partial w}{\partial y} \tag{3.23}$$

Now, the displacement components u_x and u_y are known, the components of strain tensor can be determined as

$$\epsilon_{xx} = -z\frac{\partial^2 w}{\partial x^2}, \qquad \epsilon_{yy} = -z\frac{\partial^2 w}{\partial y^2}, \qquad \epsilon_{xy} = -z\frac{\partial^2 w}{\partial x \partial y} \tag{3.24}$$

$$\epsilon_{xz} = \epsilon_{yz} = 0, \qquad \epsilon_{zz} = \frac{\nu}{1-\nu}z\left(\frac{\partial^2 w}{\partial x^2} + \frac{\partial^2 w}{\partial y^2}\right) \tag{3.25}$$

Internal stresses in a film on a substrate causes the film and substrate to bend until they reach the mechanical equilibrium, i.e. until both net force and bending moment become zero [47]. The average film stresses, $\bar{\sigma}^f$, can be determined from deformed curvature of deposited substrate. This method is very well-known to determine film stresses since the curvature of a bent substrate can be measured. Silicon and silicon nitride are widely used as the substrates because of their mechanical properties. Even though Stoney formula is generally used to find film stress, it does not cover in the case of thick film. It works well with thin film when thickness of a film is very small compared with of a substrate. Stoney formula for film stress which was first published in 1909 is given by

$$\sigma_{zz}^f \approx -\frac{h_s^2}{6h_f}\frac{1}{R}E_s \tag{3.26}$$

where R is the radius of curvature and E_s is Young's modulus of the substrate. Since Stoney formula is based on beam theory, subscript "zz" denotes the stress component in direction of the z-axis in this case.

In the case of thin films deposited on plate-like substrates, the biaxial deformation has to be taken into account by introducing the biaxial modulus, $\bar{E}_s$, of the substrate rather than only uni-axial Young's modulus.

$$\bar{E}_s = \frac{E_s}{1-\nu_s} \tag{3.27}$$

where ν_s is Poisson's ratio of the substrate.

Now, considering a plate-like substrate of arbitrary symmetry, the curvature

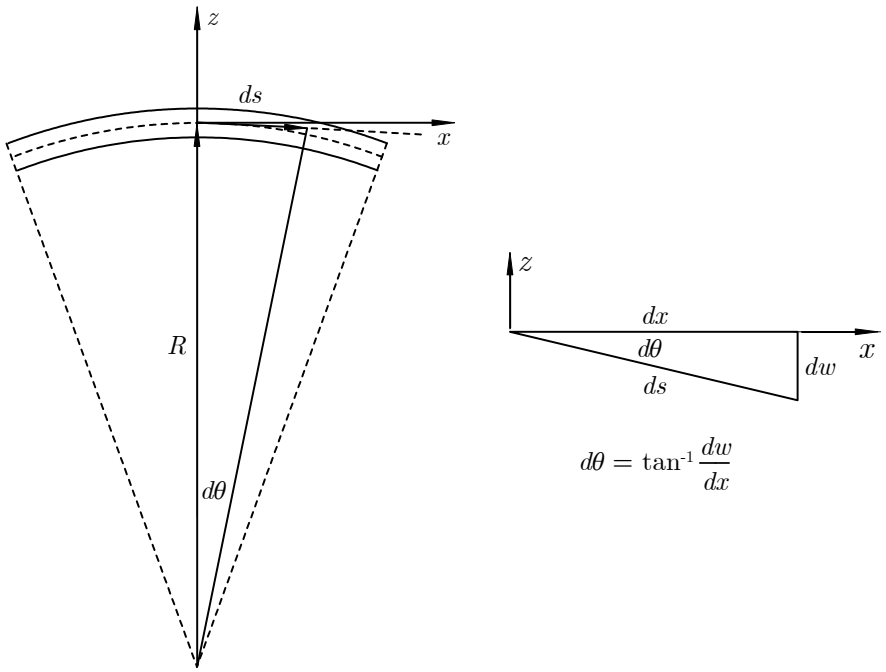

Figure 3.6: The geometry of deformation.

R of this substrate can be exactly written as

$$\frac{1}{R_x} = \frac{w''}{\left(1 + (w')^2\right)^{\frac{3}{2}}} \approx w'' \tag{3.28}$$

where $w' << 1$.

Using the plate approximation above assuming that the stress components in z-direction is very small compared to the others, so stresses in this component can be neglected.

$$\bar{\sigma}_{xz} = \bar{\sigma}_{yz} = \bar{\sigma}_{zz} = 0 \tag{3.29}$$

With the origin of the z-axis lying at the substrate bottom, the following equations for the normal deformations can be written as

$$\bar{\sigma}_{xx} = \frac{E}{(1+\nu)(1-2\nu)} \left[(1-\nu)\,\epsilon_{xx} + \nu\,(\epsilon_{yy} + \epsilon_{zz})\right] \tag{3.30}$$

$$\bar{\sigma}_{yy} = \frac{E}{(1+\nu)(1-2\nu)} \left[(1-\nu)\,\epsilon_{yy} + \nu\,(\epsilon_{zz} + \epsilon_{zz}) \right] \tag{3.31}$$

Substituting ϵ_{xx}, ϵ_{yy}, and ϵ_{zz} in terms of the plate displacement $w(x, y)$ to obtain the stress components $\bar{\sigma}_{xx}$ and $\bar{\sigma}_{yy}$

$$\bar{\sigma}_{xx} = -\frac{Ez}{(1-\nu^2)} \left(\frac{\partial^2 w}{\partial x^2} + \nu \frac{\partial^2 w}{\partial y^2} \right) \tag{3.32}$$

$$\bar{\sigma}_{yy} = -\frac{Ez}{(1-\nu^2)} \left(\frac{\partial^2 w}{\partial y^2} + \nu \frac{\partial^2 w}{\partial x^2} \right) \tag{3.33}$$

For the case of constant curvature, $\partial^2 w/\partial x^2 = \partial^2 w/\partial y^2$

$$\bar{\sigma}_{xx} = -\frac{Ez}{1-\nu} \frac{\partial^2 w}{\partial x^2}, \qquad \bar{\sigma}_{yy} = -\frac{Ez}{1-\nu} \frac{\partial^2 w}{\partial y^2} \tag{3.34}$$

Hence $\bar{\sigma}_{xx} = \bar{\sigma}_{yy}$ is a function of z only. From the general transformation rule when $\bar{\sigma}_{xy} = 0$ and $\bar{\sigma}_{rr} = \text{constant}$

$$\bar{\sigma}_{rr} = \bar{\sigma}_{xx} \cos^2 \phi + \bar{\sigma}_{yy} \sin^2 \phi + \bar{\sigma}_{xy} \sin 2\phi \tag{3.35}$$

For homogeneous stress distribution, that the sum of forces and torques within the body must be equal to zero at the equilibrium. The level of the neutral surface, $(z = a)$, can be determined by these two conditions.

Force Free Condition:

$$\begin{aligned} F &= \int_0^{h_t} \bar{\sigma}_{rr}(z) dz \\ &= \int_0^{h_s} \frac{E_s}{1-\nu_s} \frac{\partial^2 w}{\partial r^2} (z-a)\, dz + \int_{h_s}^{h_t} \bar{\sigma}^f_{rr}(z) dz = 0 \end{aligned} \tag{3.36}$$

Torque Free Condition:

$$\begin{aligned} M &= \int_0^{h_t} \bar{\sigma}_{rr}(z)\,(z-a)\, dz \\ &= \int_0^{h_s} \frac{E_s}{1-\nu_s} \frac{\partial^2 w}{\partial r^2} (z-a)^2\, dz + \int_{h_s}^{h_t} \bar{\sigma}^f_{rr}(z)\,(z-a)\, dz = 0 \end{aligned} \tag{3.37}$$

where the radial film stress $\bar{\sigma}^f_{rr}(z)$ is constant throughout the film layer. The z-axis is set at the bottom of the substrate and thus $\bar{\sigma}^s_{rr} = 0$ at the neutral surface. The total force F of the system consists of one from substrate and one from the film must be equal to zero at the equilibrium.

$$F = F_s + F_f = 0 \tag{3.38}$$

which leads to

$$\bar{\sigma}^f_{rr} = -\frac{1}{h_f}\frac{E_s}{1-\nu_s}\frac{\partial^2 w}{\partial r^2}\frac{(z-a)^2}{2}\bigg|_0^{h_s} \tag{3.39}$$

and substituting the value of $\bar{\sigma}^f_{rr}$ into the equation for torque free condtion

$$\int_0^{h_s}\frac{E_s}{1-\nu_s}\frac{\partial^2 w}{\partial r^2}(z-a)^2\,dz + \int_{h_s}^{h_t}\left(-\frac{1}{h_f}\frac{E_s}{1-\nu_s}\frac{\partial^2 w}{\partial r^2}\frac{(z-a)^2}{2}\bigg|_0^{h_s}\right)(z-a)\,dz = 0 \tag{3.40}$$

The above equation allows the location ($z = a$) of the neutral surface to be obtained as

$$a = \frac{1}{6}\frac{2h_s + 3h_f}{h_s + h_f}h_s \tag{3.41}$$

Hence, the radial film stress is obtained as

$$\bar{\sigma}^f_{rr}h_f = -\frac{E_s}{1-\nu_s}\frac{\partial^2 w}{\partial r^2}\frac{h_s^3}{6h_f(h_s+h_f)} \tag{3.42}$$

Using the approximation for the curvature, $1/R \approx \partial^2 w/\partial r^2$,

$$\bar{\sigma}^f_{rr}h_f \approx -\frac{E_s}{1-\nu_s}\frac{h_s^3}{6h_f(h_s+h_f)}\frac{1}{R} \tag{3.43}$$

For the case of thin flim $h_f/h_s << 1$, the above expression leads to the Stoney formula as

$$\bar{\sigma}^f_{rr} = -\frac{E_s}{1-\nu_s}\frac{h_s^2}{6h_f}\frac{1}{R} \tag{3.44}$$

3.6 Surface Stresses

Surface stress arises when thin films or surface atoms suppressing some dynamic microstructural process producing a change in density while these atoms are attached to their substrate [48]. Bond strengths between surface atoms and sub-surface atoms create either a tensile surface stress or a compressive surface stress depending on forces between surface atoms. A concave surface curvature is caused by attracting surface atoms, while a convex surface curvature is produced by repelling surface atoms. Also, thin film rigidly attached to the substrate would create either a tensile surface stress or a compressive surface stress at the interface between the thin film and the substrate. Surface stress results from atomistic interactions between surface atoms, intermolecular forces between absorbed molecules themselves on the substrate, temperature changes, and phase transitions. For atomistic explanation, the origin of surface stress is created by charge distribution in which of the bulk metal and of the metal surface are different. Electrons redistribute themselves when there is the absence of atoms above the surface. The electrons will then respond to the missing atoms and the electronic charge must rearrange itself. This in turn causes net forces on the surface atoms. Surface stress is then produced by these atomistic interactions between surface atoms.

Based on theoretical calculations, the surface stress depends on the crystallographic orientation of the surface and on the electronic structure of the material [49]. To define the surface stress, a plane intersecting the surface of a solid material with a right angle is considered. After the surface is cut, the atoms and the elec-

tronic charge distribution on the surface will change. Forces acting on the nuclei are induced by Coulomb forces of the changes of electronic charge density and the nuclear charges. So, to keep the mean forces acting to the nuclei on the plane balanced, there will be some forces placing on each atom in such a way that the mean position of the atoms remains unchanged. The surface stress is then defined as the sum of forces, $\vec{f}^{\nu}$, acting to the nuclei minus sum of the forces one would have to place on the atoms, $\vec{f}_b^{\nu}$, and then divided by the length l of the intersection of the cutting plane and the surface.

$$\vec{\sigma} = \frac{1}{l} \sum_{\nu} \left(\vec{f}^{\nu} - \vec{f}_b^{\nu} \right) \tag{3.45}$$

where the vector $\vec{\sigma}$ can be written into the tensor form of σ_{ij} by making reference to the orientation of the intersecting plane. Based on the definition of stresses in theory of elasticity, a normal stress component is positive when it points out in the direction of positive outward normal vector. The infinitesimal reversible work δW is defined as

$$\delta W = -A \sum_{i} \sum_{j} \sigma_{ij} \delta \epsilon_{ij} \tag{3.46}$$

where $\delta \epsilon_{ij}$ is the infinitesimal stain and is A the surface area. Also, this reversible work is equal to the infinitesimal variation in the surface free energy, $-\delta F_s$,

$$A \sum_{i} \sum_{j} \sigma_{ij} \delta \epsilon_{ij} = \delta F_s = \delta \left(\gamma A \right)$$

where γ is the surface free energy per unit area or the surface tension. Generally, atomic adsorption to a surface causes a change in the surface free energy (also, called surface tension). A change in surface stress produces the mechanical response which in this case is the bending of the microcantilever. Surface tension is

defined as the reversible work per unit area needed to create a new surface plastically, whereas the surface stress is the reversible work per unit area needed to create a new surface elastically. The new surface area of solids could be created elastically by stretching the surface while in liquid the molecules are mobile and can enter or leave a strained surface. Shuttleworth [50] defines surface stress, σ, in term of γ as

$$\sigma = \gamma + A\frac{\partial \gamma}{\partial A} \tag{3.47}$$

The second term on the right-hand side of Eq. (3.47) vanishes for a liquid, because atoms are allowed to move freely onto the surface and then the number of surface atoms per area is the same as before the expansion. So the free energy per area, γ, must therefore remain constant; clearly, this is not so for a solid surface.

3.7 Overview of Micromechanical Cantilever-Based Sensing

Microcantilevers have been used in sensing applications with high sensitivity. They are attracting a growing interest due to their capabilities for high sensitivity, low cost, simple procedure, small sample consumption and quick response. Moreover, the fabrication-technology has been developed to increase the sensitivity limit up to the extent that researchers can now visualize the counting of molecules. The commercial availability of atomic force microscope (AFM) microcantilever has been stimulated the development of various microcantilever-based sensing applications. Basic principle of these microscopes is to work by measuring a local property, such as height, optical adsorption, or magnetism-with a probe or tip placed very close

to the sample. AFM imaging is operated by scanning the tip over a surface while monitoring the cantilever deflection. These deflections arise from forces between a tip and a sample which could be either attractive or repulsive forces [7]. The deflection of the microcantilever is always monitored as it bends in response to forces acting on the tip in static mode, while the resonant frequency is monitored in dynamic mode. In many sensing applications, it is used without a tip and simply worked by using the body or surface properties to probe nanoscale phenomena.

The basic principle of microcantilevers for sensing applications is the measurement of the nanometer-scale variation of the static mode and dynamic mode of the microcantilever owing to molecular adsorption on the surface. In static mode, measurements are usually performed in liquids due to the low quality factor of microcantilevers in liquids. The mechanism for the static signal (microcantilever bending) is the buildup of differential surface stress when molecular adsorption preferentially occurs on one side of the surface. The difference of surface stress between surfaces is relaxed by unequal expansion or contraction of both surfaces, resulting in a cantilever bending.

A microcantilever is the miniaturized counterpart of a diving board moving up and down. Its dimension is in microns which is million times smaller than the diving board and it moves when a mass of analyte is adsorbed on its surface. Deflection and vibrational frequency on the microcantilevers are caused by adsorbed molecules. It can bend either up or down depending on the nature of chemical bonding of the molecules. There are different shapes of microcantilevers as shown

in Fig. 3.7.

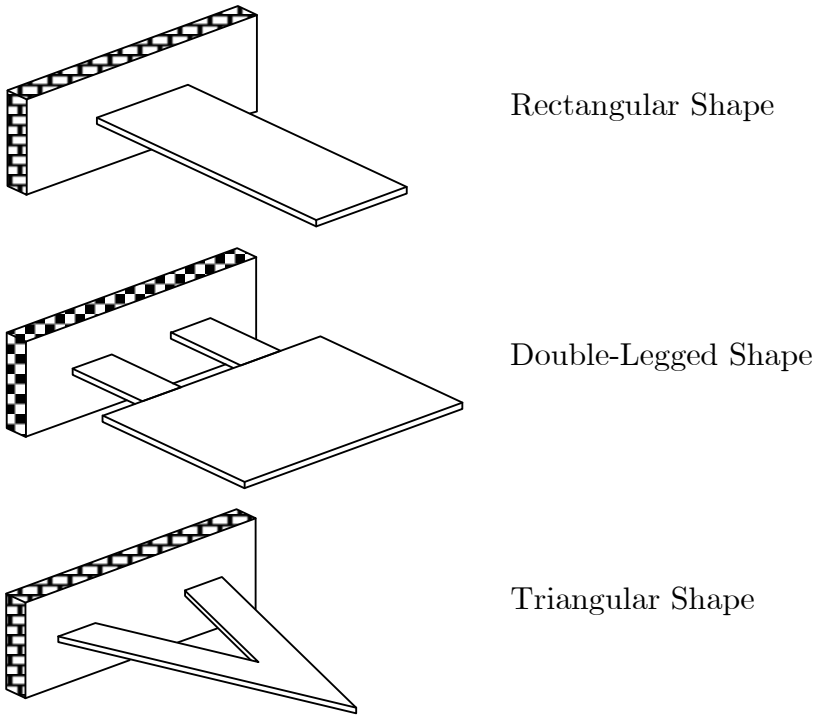

Figure 3.7: Different types of microcantilevers.

3.7.1 Mechanical Properties of Cantilever The basic mechanical properties of a cantilever are the spring constant and the resonant frequency. Based on Hooke's law, the applied force, F, to bend a cantilever is equal to spring constant, k, times resulting displacement of the cantilever, x.

$$F = -kx \tag{3.48}$$

The spring constant of a cantilever of length L is related directly to its bending stiffness EI as

$$k = \frac{3EI}{L^3} \tag{3.49}$$

where E is the Young's modulus and I is the moment of inertia (second moment of cross-section area) about the axis of bending. Hence, the resonant frequency ω_n for a cantilever can be written as

$$\omega_n = \sqrt{\frac{k}{m}} \tag{3.50}$$

The resonant frequencies of commercially available microcantilevers having the sizes of 50-400 μm range from 10-300 kHz in air.

3.7.2 Bending Behavior of a Rectangular Microcantilever

Atomistic interactions between surface atoms, intermolecular forces between adsorbed molecules, temperature changes and phase transition can produce surface stress. When absorbed molecules preferentially attaches to one surface, this causes a cantilever to bend. In between the areas of compressive stress and tensile stress, there is a neutral plane which no stresses act on that plane or no deformation occurred. The bending moment due to force F acting at a distance c from the neutral plane can be written as

$$M = Fc \tag{3.51}$$

This bending moment relates to the curvature (approximated) as

$$\frac{1}{R} = \frac{d^2z}{dx^2} = \frac{M}{EI} \tag{3.52}$$

where E is the Young's modulus and I is the moment of inertia about the axis of bending. For a rectangular cross-section area, I is given by

$$I = \frac{1}{12}wh_s^3 \tag{3.53}$$

for which w is the beam width and h_s is the beam thickness.

The bending moment of the beam caused by the differential in surface stresses is given by

$$M = \frac{1}{2} h_s w \Delta\sigma \tag{3.54}$$

where $\Delta\sigma = \sigma_1 - \sigma_2$ is the differential surface stress with σ_1 and σ_2 are surface stresses at the upper and lower surfaces of the cantilever, respectively. Substituting I and M into the equation of bending moment and the curvature above, then Stoney's formula is obtained as

$$\frac{1}{R} = \frac{6\,(1-\nu)}{E h_s^2} \Delta\sigma \tag{3.55}$$

The governing equation above is shown the relationship between the substrate's curvature and the surface stress. Next topics are about roles of microcantilvers as sensors and methods to detect their deflections.

3.8 Micromechanical Cantilevers in Sensing Applications

3.8.1 Surface Stress Sensing

Adsorption of molecules to the surface of a substrate leads to a change in surface stress which causes mechanical response, such as the bending moment of a microcantilever. The microcantilever in sensing applications is typically sensitive to a specific molecule of interest. The sensing layer is employed to the microcantilever surface to promote the adsorption of the molecules. To avoid changes in mechanical properties of the microcantilever, to generate uniform surface stress, and to avoid interactions with the solid substrate beneath, the thin, uniform and compact sensing layer is needed to be deposited [51]. To

raise surface functionalization for a sensor, a layer which is specific to molecules of interest is coated on one side of the microcantilever. For example, sensing of the self-assembled of alkanethiol monolayers on gold-coated cantilevers [19], this thin gold film acts as the sensing layer. Moreover the gold film is typically sensitive to thiol group, alkanethiols can then be anchored to the substrate causing the surface stress.

Several groups have developed the microcantilever-based sensor to probe changes in surface stress yielding its mechanical response. Wu et al. [52] have studied about microcantilever for diagnosis of cancer. Microcantilever was coated with antibodies which is specific to prostate specific antigen (PSA). A prostate cancer antigen is found in the patients having prostate cancer. When the blood sample of the patients having prostate cancer interacts with the antibodies on microcantilever, the microcantilever is bent due to absorbed antigen molecules. The very small bending of microcantilever can be detected by a low power laser beam using photodetector. This method is more sensitive than conventional biochemical techniques. An array of microfabricated cantilevers functionalized with anchored anti-creatin kinase and anti-myoglobin antibodies can be used to detect proteins which are creatin kinase and myoglobin. These proteins, creatin kinase and myoglobin, are detected via measurement of surface stress generated when antibodies on the cantilever recognize antigens. Baselt et al. [53] achieved an array of 10 micromachined cantilever beams for hydrogen sensing. Cantilevers coated with palladium-nickel bend when there is presence of hydrogen.

Moreover, this kind of sensor has been applied to detect single-nucleotide polymorphism. Mutations due to single nucleotide polymorphisms (SNPs) within the known gene sequences and the genome cause several diseases such as Alzhimer, Thallassemia's disease etc. Early detection of the single nucleotide polymorphism will aid the diagnosis and help in the treatments of patients having such disorders. Microcantilevers having high sensitivity to specific biomolecular recognition interactions have been introduced to detect single base pair mismatches in DNA. Gold coated microcantilever is attached by thiolated DNA which is specific for the particular target DNA. Complementary hybridization between thiolated DNA and target DNA drives the net positive deflection of the cantilever. In contrary, a net negative deflection of the cantilever is caused by increased repulsive forces acting on the gold-coated surface of microcantilever due to hybridization of the probe DNA (thiolated DNA) with target DNA having one or two base pair mismatches [9]. Therefore, this technology holds a great promise for the medical diagnosis.

3.8.2 Heat Sensing The heat sensing works when a microcantilever composed of materials with different thermal expansion coefficients. It can be used as precise heat sensors and calorimetry sensors by exploiting the bimetallic effect. Changes in temperature and heat bend the microcantilever. Even changes of temperature as small as 10^{-5} K can be detected by this microcantilever. In addition, microcantilevers can be used as microcalorimeters to study the heat evolution in catalytic chemical reactions and enthalpy changes at phase transitions. The microcantilever deflection results from the absorption of heat either at a localized spot on the can-

tilever or along its entire length. With very small size of a microcantilever, it can be used to measure very small amount of heat like picojoule.

3.8.3 Mass Sensing A microcantilever based mass sensing is operated by monitoring changes of a resonant frequency due to mass loading acting on the microcantilever. The basic principle of this device is increasing in mass due to molecules bind to a microcantilever causes a result of the resonant frequency decreasing. Ilic et al. [13] worked on this technique to detect *Escherichia coli* (*E. coli*) cell antibody binding on silicon nitride cantilever. Changing in mass due to the specific binding of the *E. Coli* cells was detected as a resonant frequency shift of the micromechanical oscillator. Gupta et al. [55] studied micro-fabricated arrays of silicon cantilevers as microresonator sensors with nanoscale thickness which is used to detect mass loading due to virus particles. The change in resonant frequency is a function of the virus particle mass binding on the microcantilever surface. Attogram detection by nanoelectromechanical oscillators has been studied by Ilic et al. [56]. This oscillator has very high sensitivity to detect the presence of mass loading. When a microcantilever subjects to a viscous medium around it, resonant frequency of the microcantilever oscillation decreases due to viscosity effects [12]. With a microcantilever's sensitivity and very small size, they can be used as components in biosensors.

3.8.4 Mixture Detection An array of microcantilever which is micro-fabricated has been using as a selective, ultrasensitive, quantitative, chemical sensor (artificial nose). The prototype of an artificial nose is presented by Lang et al. [57].

The mechanical response of the microcantilever is responded to chemical reactions transduced by sensitization of the microcantilever with coating such as a self-assembled monolayer, a metal or a polymer. An optical beam technique is introduced to measure the deflection. This device can be employed to detect hydrogen, primary alcohols, natural flavors and water vapor. In addition, each cantilever in a microcantilever array could be coated differently to be specific an organic compound. Microcantilevers modified with a self-assembled monolayer of triethyl-12-mercaptododecylammonium bromide are reported as a chemical sensor to detect trace amounts of CrO_4^{2-} [58]. The self-assembled monolayer was deposited on a thin layer of gold-coated microcantilever. The microcantilever bends when it undergoes sorption of ions on the monolayer-modified side. These devices could then be used for the chemical detection of a number of gaseous analytes with multiple applications in a wide range of industries. There are many examples in the medical and pharmaceutical industries such as the detection of various diseases by monitoring a patient's blood chemistry or exhaled breath. For example, the metabolic disease *diabetes mellitus* caused by a partial or total lack of insulin (Insulin promotes the source of energy, glucose, into the cell) is identified [59]. Lacking insulin and also glucose in the cell leads to increasing fat consumption to obtain the sufficient energy. The intermediated products of the fat consumption will be produced as ketones. Moreover, acetone which is one of these ketones could be found in exhaled breath and urine. Early diagnosis with very small amounts of acetones in a patient's exhaled breath is important to be detected.

3.9 Micromechanical Cantilever Deflection Detection Method

Several research groups have observed that microcantilevers can transduce a number of different signal domains e.g. mass, temperatures, heat, electromagnetic field, stress, into a mechanical deformation, either a bending or a change in the resonance frequency. Many deflection detection methods have been proposed to measure a microcantilever deflection with a very fine resolution.

3.9.1 Optical Deflection Detection Method

The optical method uses a laser beam of very low power in the range that does not affect the molecules coated on the surface of the microcantilever [51]. The visible light from this low power of laser diode is focused on the apex of the microcantilever and gets reflected at the gold layer coated on the surface. The reflected beam hits a position which is sensitive photodetector and it moves on the photodetector surface when the cantilver bends. So, the beam would fall on a particular spot on the photodetector when the cantilever is undeflected (not coated with any molecule). This device is able to detect deflection in even sub-nanometer range.

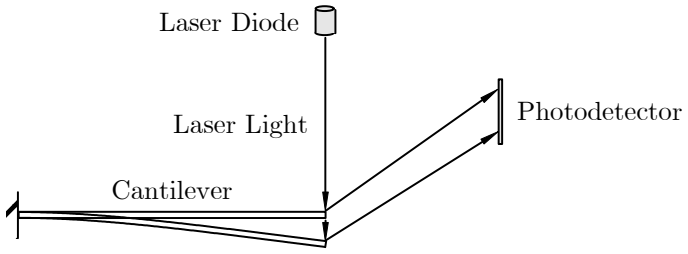

Figure 3.8: Optical deflection detection method.

3.9.2 Interferometry Deflection Detection Method The interferometry deflection detection method [60] is based on the interference between a reference laser beam and reflected laser beam on the microcantilever. Optical fiber few microns away from the free end of the microcantilever receives one part of the light reflected at the interface between fiber and surrounding media and the other part reflected at the back of the microcantilever. Interference between these two beams occurs inside the fiber and the signal can be measured by a photodiode. This method works well for small displacements but it is less sensitive in liquids.

3.9.3 The Capacitive Deflection Detection Method The capacitive method detects changes in capacitance of a plane capacitor due to the microcantilever deflection taking place when analytes adsorps on to the microcantilever. The microcantilever here is one of the two capacitor plates. This deflection technique is highly sensitive, but not suitable for measuring large displacements and not appropriate in electrolyte solutions due to the faradic currents between the capacitor plates.

3.9.4 The Piezoresistive Deflection Detection Method In this method, a piezoresistive material is embedded near the top surface of the cantilever to record the changes due to stresses occurring at the surface of the microcantilever. Stress changes due to the deflection of a microcantilever apply strain to the piezoresistor. The strain applied to the piezoresistor causes a change in resistance which can be measured by electronics methods. The location of a piezoresistor has to be close to one surface of the microcantilever to maximize the sensitivity. The piezoresistive

microcantilever associated with the Wheatstone Bridge circuit can then be used to measure a resistance change due to the microcantilever subjected to a deflection [61]. The good thing about the piezoresistive method is that the readout system can be integrated on the chip, but the deflection resolution for the system is only one nanometer which is less than the optical detection method. However, it overcomes the optical method in such a way that the optical method subjected to artifacts due to changes in the optical properties of the medium surrounding the microcantilever. The disadvantage of the piezoresistive method is due to a piezoresistor which has to be embedded in the microcantilever. So, the fabrication of such a microcantilever with a composite structure is so complicated.

Moreover, the deflection of a microcantilever could be detected by *the optical diffraction grating deflection detection method* and *the charge coupled device* (CCD) *detection method*. The first method is based on a diffraction pattern produced by reflected laser light which is proportional to the microcantilever deflection. The later method is using CCD camera to measure the deflection of the microcantilever which responds to analytes. This is like the optical method in such a way that CCD acts as the photodetector to record the laser beam deflected from the microcantilever.

CHAPTER 4

Micromechanical Cantilevers under Surface Stress Effects

As stated in the previous chapters, a micromechanical cantilever or microcantilever is generally found in Micro/Nanoelectromechanical Systems (MEMS/NEMS) because of its high sensitivity to the stimuli. One of the applications of the microcantilever is in sensing technology in which it can detect even small amount of mass or small force. Modified with a layer specific to adsorbates on one surface, the microcantilever is then actuated by the differential of surface stress between upper and lower surface due to the adsorbates favorably attached one surface more than the other. The effects of surface stress are investigated in three models: *(i)* Stoney Model (Model I), *(ii)* Axial Load Model (Model II) , and *(iii)* Uniformly Distributed Forces on the Surface (Model III). The Stoney Model considers the corresponding moment at the microcantilever's end which is caused by surface stress at the end. In the Axial Load Model, the clamping effect is taken into account. The last model of surface stress effect is designed as forces per unit area on the surface. The energy method is introduced to formulate this kind of load. Moreover the governing equation is verified its validity by comparing the results with the finite element method.

4.1 The Stoney Model for Surface Stress Loading Effects(Model I)

The surface stress is produced when a surface is elastically stretched due to the resulting strain. In the case of clean surfaces, the origin of the surface stress is

caused by the interactions between neighboring surface atoms and of those with the environment. The unequal surface stresses on both surfaces on a microcantilever result in bending. The bending cantilever with a uniform curvature radius is usually described by Stoney formula. In the Stoney formula of a microcantilever bending, the differential surface stress is the result of concentrated moment applied at the free end of the microcantilever.

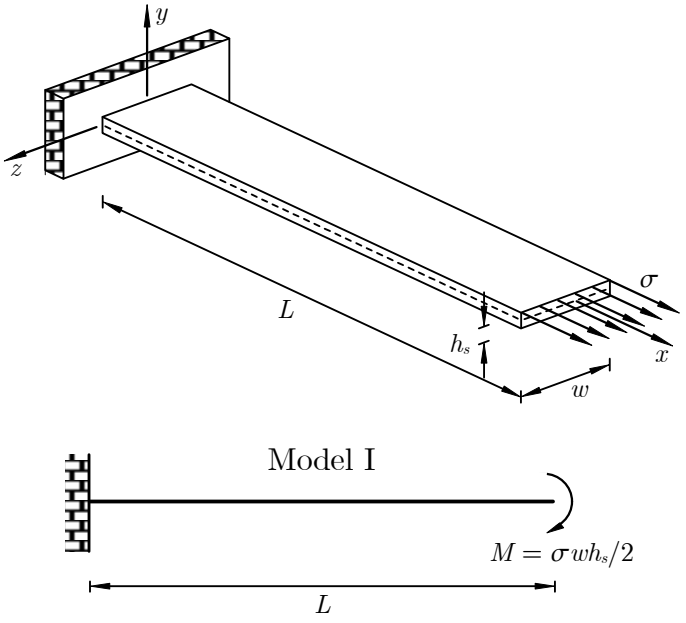

Figure 4.1: A microcantilever with a concentrated moment M applied at the free-end.

From Figure 4.1, a uniformly distributed surface loading, σ has exerted at the cantilever tip. When $\sigma > 0$, it is tensile surface stress having unit of N/m. The effect of this surface stress is designed as a concentrated moment M applied at the cantilever's free end. The governing equation of the cantilever is given as

$$-\bar{E}I\frac{d^2y}{dx^2} = M \tag{4.1}$$

where $y(x)$ is the beam defection at point x, $\bar{E}$ is the bi-axial modulus defined as $\bar{E} = E/(1-\nu)$ for which E and ν are Young's modulus and Poisson's ratio for the microcantilever, and I is the area moment of inertia. For a rectangular beam, $I = wh_s^3/12$ for which w and h_s are the beam width and thickness, respectively, M is the concentrated moment defined as $M = \sigma w h_s/2$ giving that σ is the surface stress assuming to be applied at the top surface of the cantilever. Hence, positive surface stress $\sigma > 0$ results in positive bending moment M. Equation (4.1) can be nondimensionlized by introducing the following variables variables

$$\xi = \frac{x}{L}, \qquad \eta = \frac{y}{L} \tag{4.2}$$

The nondimensional governing equation for beam displacement becomes

$$-\frac{\partial^2 \eta}{\partial \xi^2} = \frac{1}{2}\alpha\left(\beta L\right)^2 \tag{4.3}$$

where $\beta = \sqrt{\sigma w/\bar{E}I}$ and $\alpha = h_s/L$.

The boundary conditions require that

$$\eta|_{\xi=0} = 0, \qquad \left.\frac{d\eta}{d\xi}\right|_{\xi=0} = 0 \tag{4.4}$$

The displacement of the beam is easily solved by integrating the governing equation twice which leads to

$$\eta\left(\xi\right) = -\frac{1}{4}\alpha\left(\beta L\right)^2 \xi^2 \tag{4.5}$$

In the case of small deflection (linear analysis), the curvature κ of the deflected beam is approximated as $\kappa = d^2w/dx^2$. Therefore, from Eq. (4.1), the modified

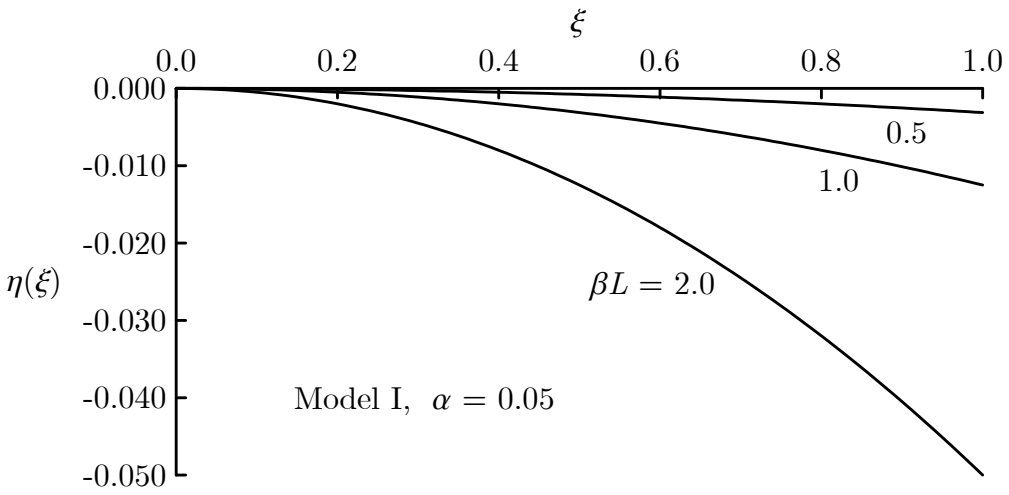

Figure 4.2: Deflections of a microcantilever using Model I for effects of surface stress under various loading parameters.

Stoney formula is given as

$$\kappa \approx \frac{1}{R} = \frac{M}{\bar{E}I} = -\frac{6\sigma}{\bar{E}h_s^2} \tag{4.6}$$

which shows that the original Stoney formula is obtained by replacing the bi-axial modulus $\bar{E}$ with Young's modulus E.

The results for beam displacement of a microcantilever with thickness to length ratio $\alpha = 0.05$ subjected to various surface stress loading parameters, βL, are shown in Fig. 4.2.

4.2 Axial Load Model for Surface Stress Loading Effects (Model II)

Since the surface stress effect based on Stoney formula takes into account of only a resultant moment applied at the end of the cantilever, the deflection is always overestimated. In this case, axial force is introduced to the governing

equation and modeled as a corresponding concentrated axial load at the free-end of the cantilever. Hence, the surface stress effect is modeled as a concentrated moment, M, and axial load, P, applied at the end.

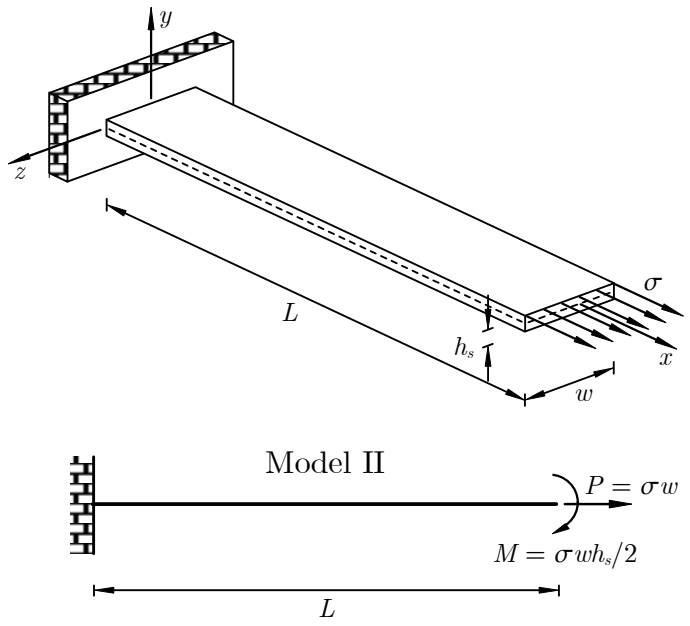

Figure 4.3: A microcantilever with a concentrated moment M and axial load P applied at the free-end.

4.2.1 Euler-Bernoulli Beam Equation In this model, the surface stress effect takes into account a corresponding concentrated bending moment M plus a corresponding concentrated axial force P at the cantilever's free-end. An axial load component is added, because one end of the microcantilever is fixed. The moment and axial force are obtained as $M = \sigma w h_s/2$ and $P = \sigma w$. From Figure 4.3, a uniformly distributed surface stress, σ, has exerted at the cantilever tip. Two methods, Euler-Bernoulli beam equation and energy method are used to analyze

the deflections of a microcantilever under this loading condition. By applying Euler-Bernoulli beam equation, the governing equation of the cantilever is given as

$$M = -\bar{E}I\frac{d^2y}{dx^2} \tag{4.7}$$

where the relations for transverse loading, $q(x)$, shear force, $V(x)$, axial force, P, and bending moment, $M(x)$, are defined as

$$\frac{dM(x)}{dx} = -V(x), \qquad \frac{dV(x)}{dx} = -q(x), \qquad V(x) = -P\frac{dy}{dx} \tag{4.8}$$

Hence, the governing differential equation for the transverse displacement $y(x)$ is obtained as

$$\bar{E}I\frac{d^4y}{dx^4} - P\frac{d^2y}{dx^2} = 0 \tag{4.9}$$

and to satisfy the following set of boundary conditions

$$y\big|_{y=0} = 0, \qquad \left.\frac{dy}{dx}\right|_{x=0} = 0 \tag{4.10}$$

$$\bar{E}I\left.\frac{d^2y}{dx^2}\right|_{x=L} + M = 0, \qquad \bar{E}I\left.\frac{d^3y}{dx^3}\right|_{x=L} - P\left.\frac{dy}{dx}\right|_{x=L} = 0 \tag{4.11}$$

To non-dimensionalize the equations, the following dimensionless variables are introduced:

$$\xi = \frac{x}{L}, \qquad \eta = \frac{y}{L} \tag{4.12}$$

and the nondimensionlized equation is given by

$$\eta'''' - (\beta L)^2\,\eta'' = 0 \tag{4.13}$$

and the corresponding set of boundary condition

$$\eta\big|_{\xi=0} = 0, \qquad \eta'\big|_{\xi=0} = 0 \tag{4.14}$$

$$\eta''|_{\xi=1} + \frac{\alpha\,(\beta L)^2}{2} = 0, \qquad \eta'''|_{\xi=1} - (\beta L)^2\,\eta'|_{\xi=1} = 0 \tag{4.15}$$

The solutions η and κ to the forth-order differential equation are obtained by direct integration as

$$\eta(\xi) = -\frac{\alpha}{2}\frac{e^{\beta L(1-\xi)}\left(-1+e^{\beta L\xi}\right)^2}{(1+e^{2\beta L})} \tag{4.16}$$

$$\kappa(\xi) = -\frac{\alpha\,(\beta L)^2}{2}\frac{e^{\beta L(1-\xi)}\left(1+e^{2\beta L\xi}\right)}{(1+e^{2\beta L})} \tag{4.17}$$

4.2.2 Energy Method In a system which conserves energy, useful insights can be obtained from some fundamental properties of the total potential energy of a system in equilibrium. A concept called the Principle of Virtual Work is introduced to predict these properties in the system. At equilibrium if a body subjecting to a combination of surface forces f_s and body forces (such as gravity) f_b deforms quasi-statically and displaces as a result of those forces, then the total work done by the external forces must equal the internal stored energy in the deformed and displaced state. The Principle of Virtual Work is like the principle that energy is conserved since only quasi-static displacements and deformations are considered without kinetic energy in the system. But in Principle of Virtual Work, the functions describing the displacements and deformations are variable to get a minimum of energy. These displacements occurs, termed virtual displacement, need not actually take place and need not be infinitesimal. But assuming the infinitesimal displacements are usually done as the system of forces is unchanged.

The symbol δ denotes a virtual infinitesimally small quantity. Consider a point in an elastic body that is unconstrained and free to experience arbitrary virtual

displacements, δu, δv, and δw, in the x-, y-, z-direction, respectively, then the virtual work accompanying these displacements is $\sum F_x \delta u$, $\sum F_y \delta v$, and $\sum F_z \delta w$ where $\sum F_x$, $\sum F_y$, and $\sum F_z$ are the force resultants in the x-, y-, z-direction, respectively. If the particle is in equilibrium, the virtual work must vanish, since $\sum F_x = \sum F_y = \sum F_z = 0$.

However, for an elastic body, it is required a number of restrictions on the arbitrary virtual displacements. These displacements have to be continuous and their derivatives have to exist. In addition, material continuity is guaranteed. Because certain displacements on the boundary may be determined by the boundary conditions while the virtual displacements at such points on the boundary must be zero. A virtual displacement does not result in the magnitude or direction of external and internal forces, but it results in an increment of the strain field on an elastic body.

The virtual strains are obtained by replacing the displacements u, v, and w by the virtual displacements δu, δv, and δw in the strain-displacement relations

$$\delta\epsilon_{xx} = \frac{\partial \delta u}{\partial x}, \quad \delta\epsilon_{yy} = \frac{\partial \delta v}{\partial y}, \quad \delta\gamma_{xy} = \frac{\partial \delta u}{\partial y} + \frac{\partial \delta v}{\partial x} \tag{4.18}$$

The elastic strain energy stored in an entire body is determined by integrating over the original or undeformed volume V.

$$U = \int_V U_0 dV = \int\int\int U_0 dx dy dz \tag{4.19}$$

where U_0 is the strain energy density such that

$$\epsilon_{ij} = \frac{\partial U_0(\sigma_{kl})}{\partial \sigma_{ij}}, \qquad \sigma_{ij} = \frac{\partial U_0(\epsilon_{kl})}{\partial \epsilon_{ij}}, \tag{4.20}$$

where ϵ_{ij} and σ_{ij} are the components of strain and stress tensors, respectively.

The variation of strain energy due to virtual strains of a elastic body that has volume V is

$$\delta U = \int_V \left(\sigma_{xx}\delta\epsilon_{xx} + \sigma_{yy}\delta\epsilon_{yy} + \sigma_{zz}\delta\epsilon_{zz} + \sigma_{xy}\delta\gamma_{xy} + \sigma_{xz}\delta\gamma_{xz} + \sigma_{yz}\delta\gamma_{yz}\right) dV \quad (4.21)$$

The virtual work done in an elastic body by the mutual actions between the infinitesimal elements in the body due to the virtual displacements is $-\delta U$. The external forces of the body experiencing virtual displacements δu, δv, and δw, therefore the virtual work done by applied forces which are body forces (F_x, F_y, F_z) per unit volume and surface forces (p_x, p_y, p_z) per unit area is

$$\delta W = \int_V \left(F_x\delta u + F_y\delta v + F_z\delta w\right) dV + \int_A \left(p_x\delta u + p_y\delta v + p_z\delta w\right) dA \quad (4.22)$$

where A is the surface area bounding the volume V.

Since the total work done during the virtual displacement is zero, $\delta W - \delta U = 0$, the principle of virtual work for an elastic body can be expressed as

$$\delta W = \delta U \quad (4.23)$$

The above equation may be rewritten as

$$\begin{aligned} \delta\Pi &= \delta\left(U - W\right) \\ &= \delta\left(U - \int_A \left(p_x u + p_y v + p_z w\right) dA - \int_V \left(F_x u + F_y v + F_z w\right) dV\right) = 0 \end{aligned} \quad (4.24)$$

The term $\Pi = U - W$ is called the potential energy. The equation above shows a condition of stationary potential energy of the system. The potential

energy is a minimum at the stable equilibrium. But displacements have to satisfy the boundary conditions. The condition at the equilibrium is that Π is a minimum value. Here it is called the principle of minimum potential energy.

The Euler-Lagrange Equation is obtained by minimization of the potential energy as shown as following:

$$\int_{x_0}^{x_1} \left(\frac{\partial F}{\partial y} - \frac{d}{dx}\frac{\partial F}{\partial y'} + \frac{d^2}{dx^2}\frac{\partial F}{\partial y''} \right) \phi dx \tag{4.25}$$

where F is a function of (x, y, y', y'') and ϕ is an admissible variation which is a function of x.

Hence, another method to obtain the governing equation of the axial load model is the energy method which is introduced in order to simplify the derivation of the equations in elastic beams and plates. If the elastic beam is bent slightly and let it go. It returns to its flat configuration and resists bending. The energy of an unloaded static beam denoted as Π [64]

$$\Pi = \Pi_S + \Pi_B \tag{4.26}$$

where Π_S and Π_B are the stretching and bending energies respectively, and are defined as

$$\Pi_S = P\left(\int_0^L \sqrt{1 + y'^2} dx - L \right), \quad \Pi_B = \frac{\bar{E}I}{2} \int_0^L y''^2 dx \tag{4.27}$$

where P is the axial force, $\bar{E}I$ is the bending stiffness and L is the length of the beam while $y' = \partial y/dx$ and $y'' = \partial^2 y/dx^2$.

The stretching energy Π_S can be approximated by the Taylor's series as

$$\Pi_S = \frac{P}{2} \int_0^L y'^2 dx \tag{4.28}$$

Hence, for the beam under small deformation

$$\Pi = \frac{1}{2}\int_0^L \left(Py'^2 + \bar{E}Iy''^2\right) dx \tag{4.29}$$

Comparing the above equation to the Euler-Lagrange equation

$$F(x, y, y', y'') = \frac{1}{2}\left(Py'^2 + \bar{E}Iy''^2\right) \tag{4.30}$$

The governing equation for beam displacement is obtained by applying the principle of minimum potential energy to the Euler-Lagrange equation for the beam

$$\bar{E}Iy'''' - Py'' = 0 \tag{4.31}$$

and is to satisfy the boundary conditions

$$y|_{x=0} = 0, \quad y'|_{x=0} = 0, \quad \bar{E}Iy''\big|_{x=L} + M = 0 \quad \bar{E}Iy'''\big|_{x=L} - P\, y'|_{x=L} = 0 \tag{4.32}$$

Introducing the nondimensional variables $\xi = x/L$ and $\eta = y/L$ and considering the parameters $\beta = \sqrt{\sigma w/\bar{E}I} = \sqrt{P/\bar{E}I}$ and $\alpha = h_s/L$, the following nondimensional forth-order ordinary differential equation is obtained as

$$\eta'''' - (\beta L)^2 \eta'' = 0 \tag{4.33}$$

and the set of nondimensional boundary conditons

$$\eta|_{\xi=0} = 0, \quad \eta'|_{\xi=0} = 0 \tag{4.34}$$

$$\eta''|_{\xi=1} + \frac{\alpha\,(\beta L)^2}{2} = 0, \qquad \eta'''|_{\xi=1} - (\beta L)^2\, \eta'|_{\xi=1} = 0 \tag{4.35}$$

The solutions for the displacement of the beam are obtained by method of integration

$$\eta(\xi) = -\frac{\alpha}{2}\frac{e^{\beta L(1-\xi)}\left(-1 + e^{\beta L\xi}\right)^2}{(1 + e^{2\beta L})} \tag{4.36}$$

$$\kappa(\xi) = -\frac{\alpha\,(\beta L)^2}{2}\frac{e^{\beta L(1-\xi)}\left(1+e^{2\beta L\xi}\right)}{(1+e^{2\beta L})} \tag{4.37}$$

Figure 4.4 shows the plots of resulting displacements for a microcantilever with thickness to length ratio $\alpha = 0.05$ and subjected to various surface stress loading parameters (βL), obtained by modeling surface stress effects by a concentrated moment and a concentrated force applied at the free-end of the cantilever (Model II).

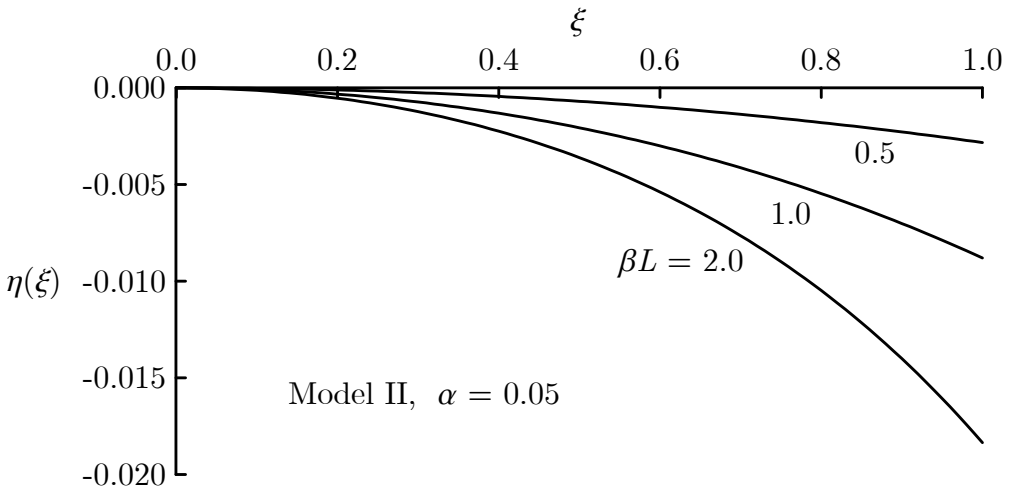

Figure 4.4: Deflections of a microcantilever using Model II for effects of surface stress under various loading parameters.

4.3 Surface Force Model for Surface Stress Loading Effects(Model III)

As the surface stress is mentioned in previous chapter, its origin could be described as intermolecular forces between atoms or molecules in the surface layer. Therefore the microcantilever could bend upward or downward depending on the forces between atoms in the layer. Hence bond strengths between surface atoms

could produce either a tensile surface stress or compressive surface stress. Attraction forces between surface atoms create a concave surface curvature. While surface atoms repel each other, this results in a convex surface curvature. Then designing surface stresses as a uniformly distributed loads acting along the beam would yield a better model of surface stress effect. These distributed loads produce a corresponding uniformly distributed axial stress and bending moment per unit length along the microcantilever.

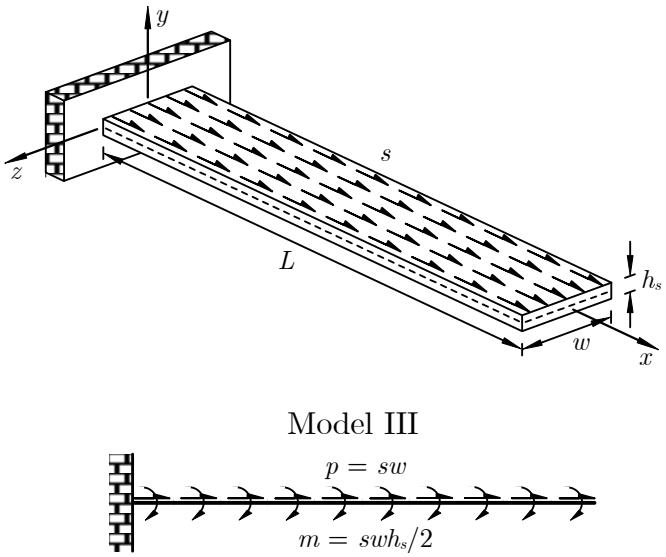

Figure 4.5: A microcantilever with uniformly distributed axial force p and uniformly distributed moment m.

4.3.1 Energy Method The principle of virtual work is introduced to derive the governing equation for beam deflection subjected to the third model for surface stress effect (Model III) and its corresponding boundary conditions.

Let W be the external work done and U be the strain energy. Since the total

work done during the virtual displacement is zero, $\delta\left(W-U\right)=0$, the principle of virtual work for an elastic body can be expressed as

$$\delta W=\delta U=\delta U_N+\delta U_V+\delta U_M \tag{4.38}$$

where U_N, U_V, and U_M are strain energies resulting from axial loading, N, shear loading, V, and bending moment, M, respectively, and are defined as

$$U_N = \int_0^L \frac{N^2}{2\bar{E}A}dx=\int_0^L \frac{1}{2\bar{E}A}\left(sw\left(L-x\right)\cos y'\right)^2 dx \tag{4.39}$$

$$U_V = \int_0^L \frac{kV^2}{2GA}dx=\int_0^L \frac{k}{2GA}\left(sw\left(L-x\right)\sin y'\right)^2 dx \tag{4.40}$$

$$U_M = \int_0^L \frac{M^2}{2\bar{E}I}dx=\int_0^L \frac{\bar{E}I}{2}\left(y''\right)^2 dx \tag{4.41}$$

where s is the applied surface force uniformly distributed along the length of the beam, w is the width of the cross-section, A is the cross-sectiona area, I is the moment of inertia about the axis of bending, $\bar{E}$ is the bi-axial modulus, and G is the modulus of rigidity.

For small deformation, $y'=dy/dx<<1$, the following approximations $\sin y'\approx y'$ and $\cos y'\approx 1$ are made. Hence

$$U_N=\int_0^L \frac{1}{2\bar{E}A}\left(sw\left(L-x\right)\right)^2 dx, \qquad U_V=\int_0^L \frac{k}{2GA}\left(sw\left(L-x\right)y'\right)^2 dx \tag{4.42}$$

The external work done due to moment is

$$W=\int_0^L m\left(L-x\right)\frac{d^2y}{dx^2}dx \tag{4.43}$$

Hence, from the Principle of Virtual Work such that $\delta(U-W)=\delta\Pi=0$

$$\Pi=\int_0^L\left(\frac{\bar{E}Iy''^2}{2}+\frac{\left(sw\left(L-x\right)\right)^2}{2\bar{E}A}+\frac{k\left(sw\left(L-x\right)y'\right)^2}{2GA}-m\left(L-x\right)y''\right)dx \tag{4.44}$$

Introducing the Euler-Lagrange Equation

$$\frac{\partial F}{\partial y} - \frac{d}{dx}\frac{\partial F}{\partial y'} + \frac{d^2}{dx^2}\frac{\partial F}{\partial y''} = 0 \tag{4.45}$$

where the function F to be minimized is defined as

$$F = \frac{\bar{E}Iy''^2}{2} + \frac{\left(sw\left(L-x\right)\right)^2}{2\bar{E}A} + \frac{k\left(sw\left(L-x\right)y'\right)^2}{2GA} - m\left(L-x\right)y'' \tag{4.46}$$

This leads to the governing differential equation for the displacement function for a microcantilever subjected to Model III surface stress loading as

$$\bar{E}I\frac{d^4y}{dx^4} - \frac{k\left(sw\right)^2}{GA}\left[\left(L-x\right)^2\frac{d^2y}{dx^2} - 2\left(L-x\right)\frac{dy}{dx}\right] = 0 \tag{4.47}$$

and the boundary equation

$$\left(\frac{\partial F}{\partial y'} - \frac{d}{dx}\frac{\partial F}{\partial y''}\right)\Bigg|_{x_0}^{x_1} + \frac{\partial F}{\partial y''}\Bigg|_{x_0}^{x_1} = 0 \tag{4.48}$$

Hence, this leads to the following proper set of boundary conditions

$$y|_{x=0} = 0, \quad y'|_{x=0} = 0, \quad \bar{E}Iy''\big|_{x=L} = 0, \quad \bar{E}Iy'''\big|_{x=L} + m = 0 \tag{4.49}$$

Introducing nondimensional variables $\xi = x/L$ and $\eta = y/L$, the dimensionless differentail equation is onbtained as

$$\frac{d^4\eta}{d\xi^4} - \frac{k\left(1+\nu\right)}{6\left(1-\nu\right)}\left(\beta L\right)^4\alpha^2\left(\left(1-\xi\right)^2\frac{d^2\eta}{d\xi^2} - 2\left(1-\xi\right)\frac{d\eta}{d\xi}\right) = 0 \tag{4.50}$$

and the corresponding boundary conditions

$$\eta|_{\xi=0} = 0, \quad \eta'|_{\xi=0} = 0, \quad \eta''|_{\xi=1} = 0, \quad \eta'''|_{\xi=1} - \frac{\alpha\left(\beta L\right)^2}{2} = 0 \tag{4.51}$$

The effect of forces ($\mathrm{N/m^2}$) uniformly distributed on the upper surface of the microcantilever has been studied. The principle of virtual work is applied to derive

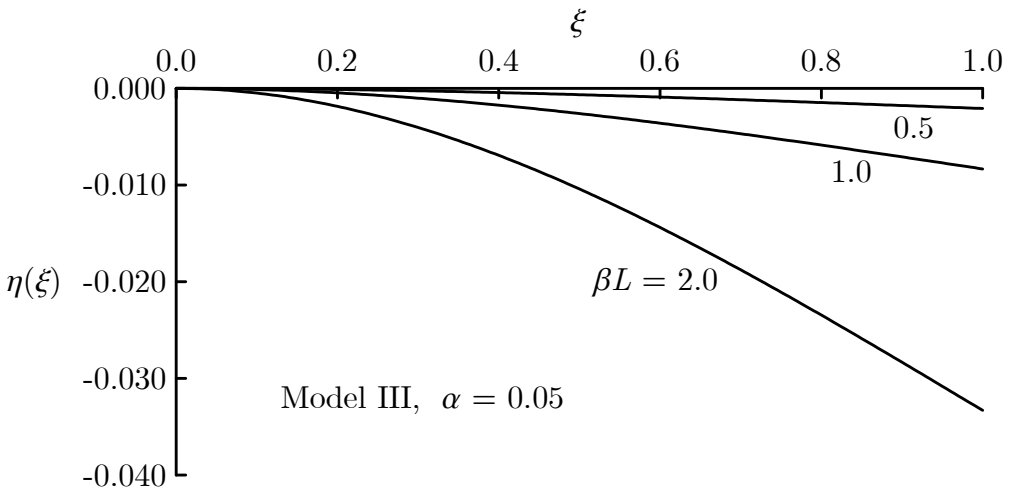

Figure 4.6: Deflections of a microcantilever using Model III for effects of surface stress under various loading parameters.

the governing equation and boundary conditions. Since the equation governing the third model is much more complicated than previous two models, the numerical method is introduced to solve this non-constant coefficient differential equation under different loading conditions. Using $E = 165$ GPa, $\nu = 0.22$, and $k = 1.2$, Figure 4.6 shows microcantilever deflections predited by Model III for surface stress loading parameters $\beta L = 0.5$, 1.0, and 2.0.

4.3.2 Finite Element Method The physical phenomena such as biology, geology and mechanics could be formulated in mathematical forms which might be algebraic equations, differential equations, or integral equations which are obtained by employing the laws of physics [66, 67]. There are two major stages for studying the physical phenomena: first one is the mathematical formulation and the second one is analyzing the mathematical model by introducing numerical methods.

The formulated mathematical forms usually appear as differential equations. Some assumptions might need to simplify the complicated physical phenomena and to develop suitable mathematical models. Numerical methods are then employed to understand and figure out the physical processes.

The governing equations are sometimes hard to find analytical solutions, so it Is easier to get the solutions approximately by numerical methods. Numerical methods basically transform differential equations which govern a continuum to a set of algebraic equations of a discrete model of the continuum. There are a number of numerical methods developed to solve equations. Generally, finite difference and variational methods are effective ways to solve the problems. In the finite difference approximation of a differential equation, the function is expanded in a Taylor series which have the values of the solution at discrete mesh points of the domain. The solutions at the mesh points to the resulting algebraic equations are obtained after applying the boundary conditions. Examples of variational methods are the Galerkin, the Ritz, collocation, and least squares methods. They are different from each other in the integral form, weight functions, and/or approximation functions. The approximate solutions of the governing equations could be assumed to be a linear combination of approximation functions with unknown coefficients. Also the equations could be written in terms of equivalent weighted-integral forms. By employing this method in the differential equations, unknown coefficients are determined when the approximated integral form must be equivalent to the governing differential equation. These traditional variational methods (meshless methods)

are not effective in the problems dealing with an arbitrary domain, because the approximation functions for the problems are difficult to construct.

The difficulty of constructing the approximation functions by the traditional variational methods can be overcome by the finite element method which is powerful to apply to real-world problems with complicated physics, geometry and/or boundary conditions. The finite element method divides a given domain into subdomains called finite elements and then an approximation solution to the problem is determined over each element. This method allows accurate representation of complicated geometry and enables easy representation of the nodal solution by functions defined in each element. Over each element, an approximated solution is a linear combination of nodal values and the whole solution is determined by assembling elements.

Since the origins of a surface stress could be thought as the interactions between molecules on the surface of the beam, these forces might be assumed as distributed load along the upper surface of the beam. With a beam fixed at one end and subjected to uniform loading on its surface, to solve this problem analytically is intractable. Therefore a numerical method is an effective way to get solutions. Among various types of numerical methods, the finite element method is considered as an accurate and powerful method. In the finite element method, interpolation theory is employed to approximate solutions of each element subdivided from the domain. Imposed boundary conditions and assembling all subdivided elements, numerical solutions by the finite element method is obtained.

In the Euler-Bernoulli beam theory, the plane sections are assumed to be perpendicular to the axis of the beam before and after deformation. The transverse deflection y of the beam is governed by the fourth-order differential equation. In finite element method, the beam is basically divided into a set of N elements. These numbers of elements are dictated by the geometry, loading, and material properties. Each element is governed the element equation which is the weak form of the differential equation. Weak forms in solid mechanics could be determined from the principle of virtual work or the governing differential equations. Boundary terms are the essential (geometric) boundary conditions involving the specification of the deflection y and slope dy/dx and the natural (force) boundary conditions are specified the values of the bending moment EId^2y/dx^2 and shear force EId^3y/dx^3 at the end points of the beam. The suitable interpolation functions have been implemented in the weak form. By substituting the finite element interpolation for the weight function into the weak form, the finite element model of the Euler-Bernoulli beam is obtained. Stiffness matrix and force vector for beam elements are assembled and then imposed boundary conditions. The resulting equations are solved for the unknown nodal displacements and forces. In this study the deflection of a micromechanical cantilever under uniformly load on the upper surface is determined numerically by the finite element method.

Here, a micromechanical cantilever made of silicon is considered. It has the thickness to length ratio $\alpha = h_s/L = 0.05$ and material properties Young's modulus $E = 165$ GPa and Poisson's ratio $\nu = 0.22$.

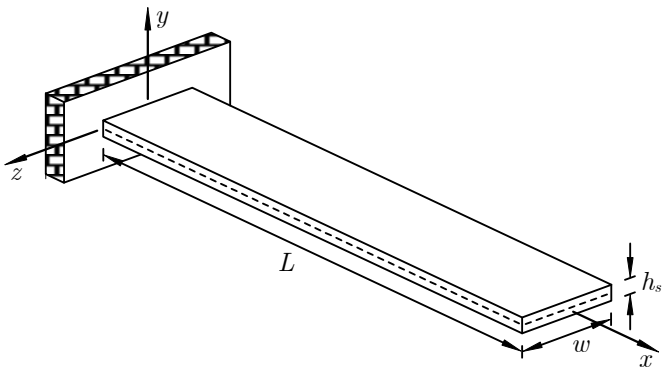

Figure 4.7: Schematic of a micromechanical cantilever.

Table 4.1: Relationship between loading parameter and force per unit area

Loading Parameter, βL	Force per Unit Area, s (N/m^2)
0.5	0.5509×10^6
1.0	2.2035×10^6
2.0	8.8141×10^6

Table 4.2: Comparison of tip-displacements by Model III and Finite Element Method

βL	Model III	Finite Element Method
0.5	-2.083×10^{-3}	-2.107×10^{-3}
1.0	-8.334×10^{-3}	-8.425×10^{-3}
2.0	-33.36×10^{-3}	-33.71×10^{-3}

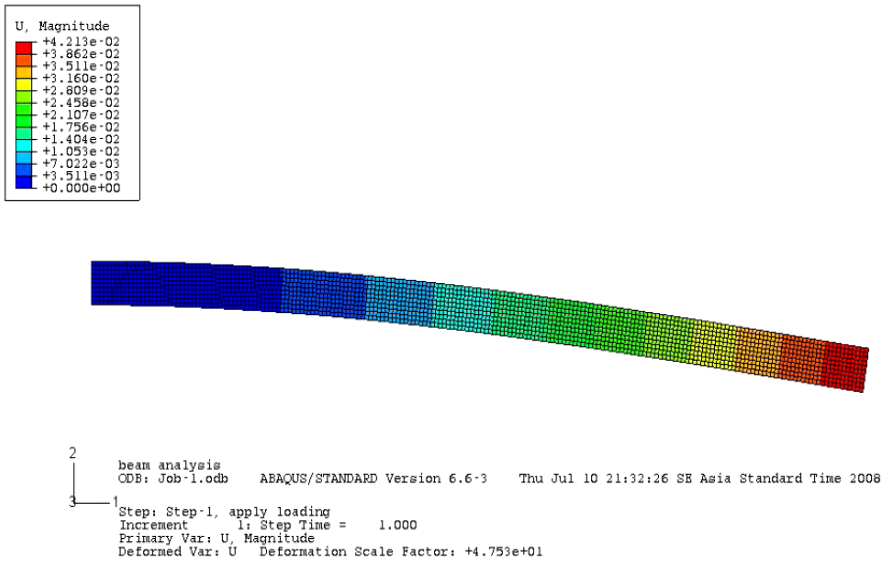

Figure 4.8: An ABAQUS result of a microcantilever subjected to surface stress loading parameter $\beta L = 0.5$.

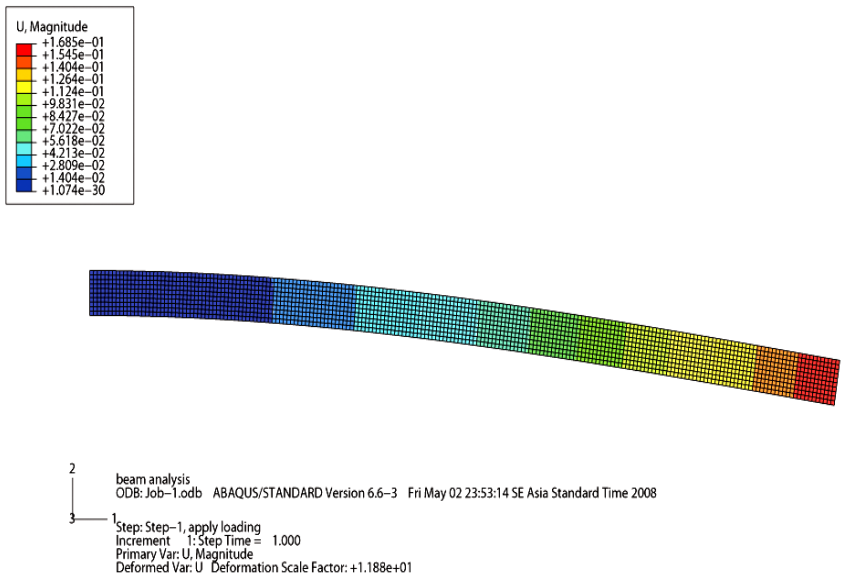

Figure 4.9: An ABAQUS result of a microcantilever subjected to surface stress loading parameter $\beta L = 1.0$.

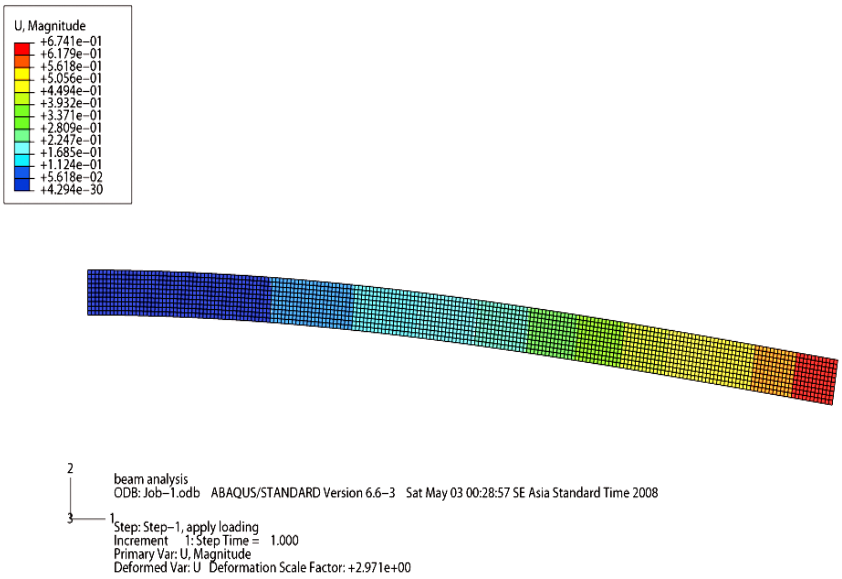

Figure 4.10: An ABAQUS result of a microcantilever subjected to surface stress loading parameter $\beta L = 2.0$.

4.4 Comparisons of Microcantilever Deflections by the Three Models

The surface stress effects according to proposed models are compared under surface loading parameters $\beta L = 0.5$, 1.0, and 2.0, respectively. In this case, model I is based on the Stoney model in such a way that concentrated moment applied at the free end of the microcantilever is considered. The second model takes into account the clamping effect corresponding to axial load model. In the third model, uniformly distributed forces on the microcantilever surface are modeled as the surface stress effects. Dimensionless deflections under the same amount of loading conditions for the three models are compared in Table 4.3. Moreover, the plots of the corresponding deflections are shown in Figs. 4.11, 4.12, and 4.13.

Table 4.3: Comparison of tip-deflection by the three models under various loading parameters

βL	Model I	Model II	Model III
0.5	-3.125×10^{-3}	-2.830×10^{-3}	-2.083×10^{-3}
1.0	-12.50×10^{-3}	-8.799×10^{-3}	-8.334×10^{-3}
2.0	-50.00×10^{-3}	-18.36×10^{-3}	-33.36×10^{-3}

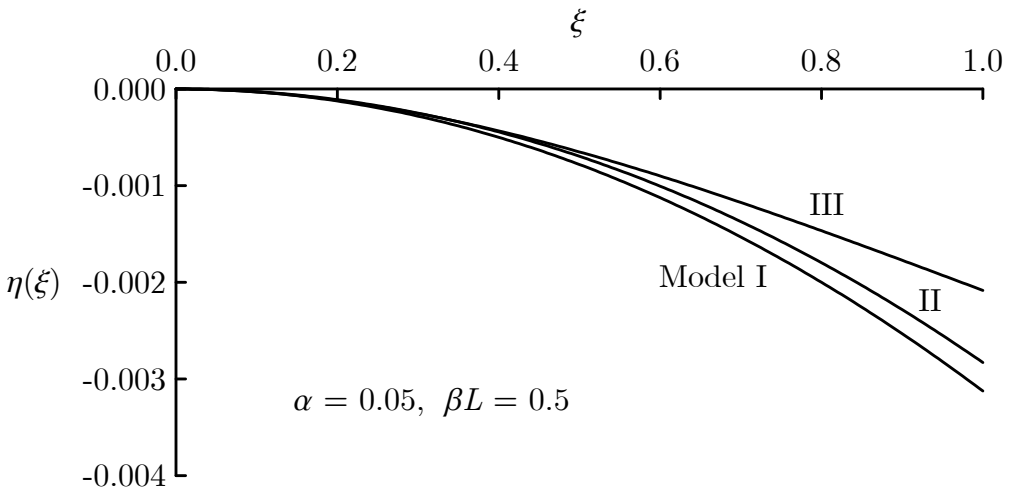

Figure 4.11: Comparison of microcantilever deflections by the three models under loading parameter $\beta L = 0.5$.

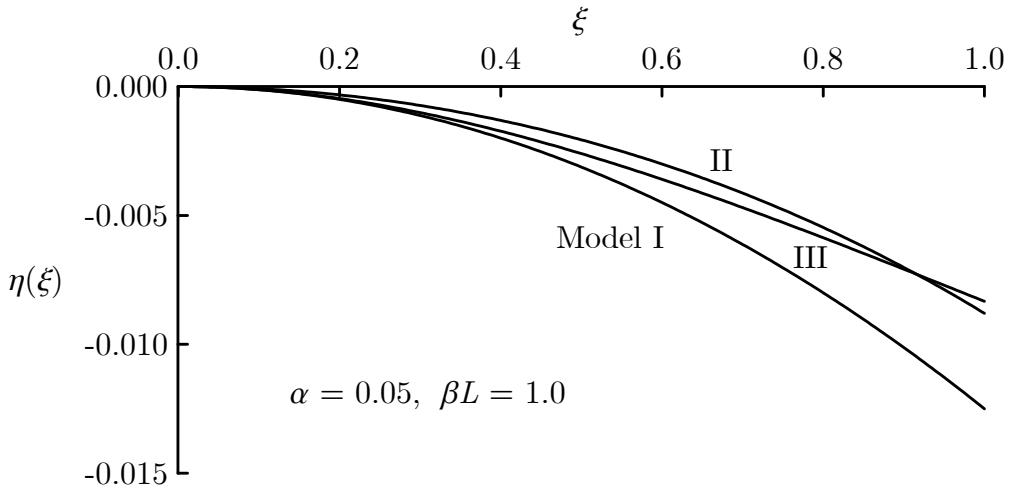

Figure 4.12: Comparison of microcantilever deflections by the three models under loading parameter $\beta L = 1.0$.

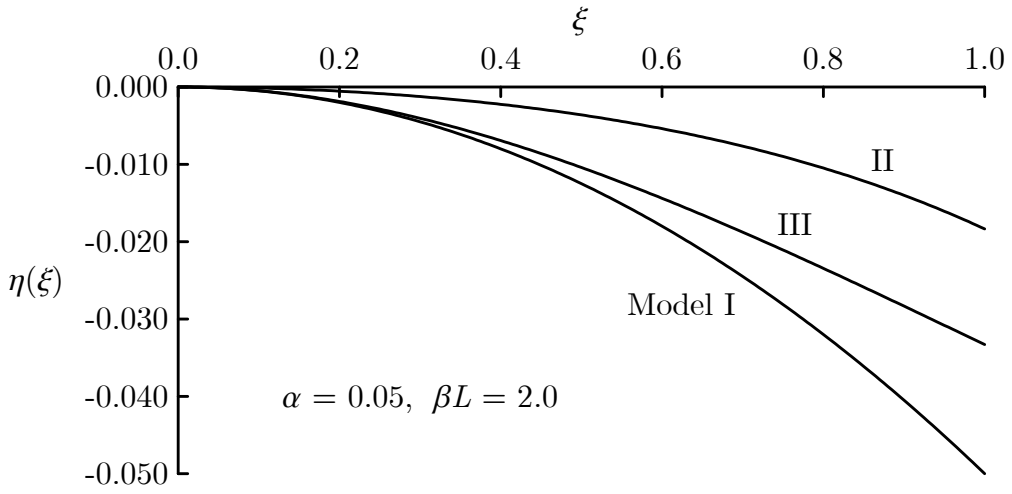

Figure 4.13: Comparison of microcantilever deflections by the three models under loading parameter $\beta L = 2.0$.

4.5 Atomistic Simulation on a Micromechanical Cantilever

Molecular forces are natural interactions due to effects happening at the subatomic level. The nature of these interactions is due to complicated effects taking place at the subatomic level which are responsible for chemical properties such as valence and bond energy. Also, the effects are accountable for the spatial arrangement (topology) of the interatomic bonds, their formation and breakage. In Molecular Dynamics (MD) computer simulation, the classical interatomic potentials should accurately account for the quantum effects to obtain reliable results. In general, the potential function is obtained from experimental observations, including from the quantum scale modeling and simulation. The general structure of this function can be presented as following [68]:

$$U\left(\vec{r}_1, \vec{r}_2, \vec{r}_3\right) = \sum_i V_1\left(\vec{r}_i\right) + \sum_{i,j>i} V_2\left(\vec{r}_i, \vec{r}_j\right) + \sum_{i,j>i,k>j} V_3\left(\vec{r}_i, \vec{r}_j, \vec{r}_k\right) + \cdots \qquad (4.52)$$

where $\vec{r}_i,\ i = 1, 2, 3$ are the radius vectors of the particles and the function V_m is called the m-body potential. The first term is the energy due to an external force field, such as gravity or electrostatic, which the system is immersed in or bounding fields, such as potential barriers and wells. The second term represents potential energy of pair-wise interaction of the particles, whereas the third term shows potential energy of the three-body components, and so on. Consequently, V_1 the function is called the external potential, V_2 "the interatomic (pair-wise) potential", and V_m, $m > 2$ "a multibody potential". In order to make numerical simulations simpler, it is practical to neglect the sum in Eq. (4.57) after the second term and incorporate all the multibody effects into V_2 with some appropriate degree

of accuracy.

4.5.1 External Fields The effect of external fields for a particle i can be commonly described as

$$V_1 = V_1(\vec{r}_i) \tag{4.53}$$

where V_1 is a function of the radius vectors of this particle. Accordingly, the instantaneous force exerted on this particle due to V_1 depends only on the spatial location of this particular particle and is independent of the positions of any other particles in the system. The following is a simple example of the potential in the uniform field of gravity

$$V_G(\vec{r}) = mgr \tag{4.54}$$

where x is the component of the radius vector, orthogonal to the earth's surface. Whereas the field of a one-dimensional harmonic oscillator is

$$V_h(x) = kx^2 \tag{4.55}$$

and a spherical oscillator

$$V_h(r) = kr^2, \qquad r^2 = x^2 + y^2 + z^2 \tag{4.56}$$

The examples of one-body interaction in the external bounding fields and potential barriers are shown as following:

A one-dimensional potential well

$$V_w(x) = -\Delta E \exp\left[-\frac{(x - x_0)^s}{2R^s}\right] \tag{4.57}$$

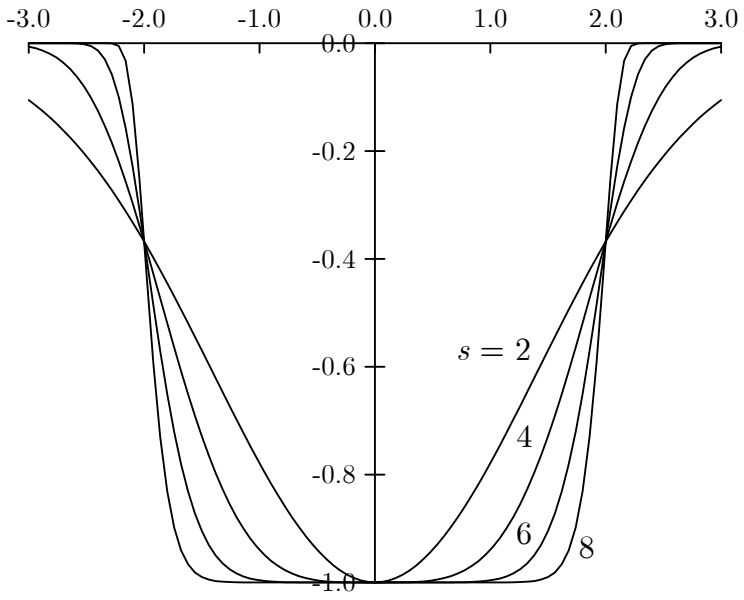

Figure 4.14: One-dimensional potential well at $x_0 = 0$, $R = 1$ with various s.

and a two-sided potential barrier

$$V_B(x) = -V_w(x) \tag{4.58}$$

where x_0, $2R$, s, and ΔE are the coordinates of the center, width, steepness and total depth/height of the well/barrier, respectively.

Three-dimensional extension for Eq. 4.57 is the 3D (parallelepiped) box

$$V_w(\vec{r}) = V_w(x, y, z) = -\Delta E \exp\left[-\frac{(x - x_0)^s}{2R_x^s} - \frac{(y - y_0)^s}{2R_y^s} - \frac{(z - z_0)^s}{2R_z^s}\right] \tag{4.59}$$

with $2R_x$, $2R_y$, and $2R_z$ are the linear dimensions of the box and the spherical chamber has its radius R and centered at $x_0 = y_0 = z_0 = 0$

$$V_w(r) = -\Delta E \exp\left[-\frac{r^s}{2R^s}\right], \qquad r = \sqrt{x^2 + y^2 + z^2} \tag{4.60}$$

Cylindrical and ellipsoidal chamber shapes can be obtained by manipulating these functions. If ΔE is increasingly large compared with an average kinetic

energy of particles, a function V_w called a "wall function" will models a system of the particles inside a vessel with impenetrable walls.

Potential wells and barriers are generally introduced to confine the spatial domain occupied by a finite system of atoms and molecules in gas or liquid phase.

4.5.2 Pair-Wise Interaction The pair-wise potential function V_2 describes the dependence of the total potential energy U on the distance between two particles. By taking $\vec{r}_i$ and $\vec{r}_j$ as the radius vectors of two arbitrary particles in the system, the potential could be written as

$$V_2\left(\vec{r}_i, \vec{r}_j\right) = V_2\left(\vec{r}\right), \qquad r_{ij} = |\vec{r}_{ij}| = |\vec{r}_i - \vec{r}_j| \tag{4.61}$$

This function serves as an addition to V_1 in Eq. (4.52) providing the dependence of U only on the radius vectors $\vec{r}_i$ and $\vec{r}_j$. Basically, there are two major types of pair-wise interactions which are long-range electrostatic interactions and short-range interactions between electrically neutral particles.

Long-range Coulomb interaction One of the basic physical characteristics of atoms and molecules is the electric charge, e. Electric charge is associated to the property of particles in such a way that it exerts forces on each other by means of electric fields. The standard SI unit of electric charge is 1 Coulomb, $e = 1$ C. The electric charge of a particle is always quantized that occurs as a multiple of the elementary charge $e_0 = 1.602177 \times 10^{-19}$ C. An electron, proton and neutron, the atomic components, have the charges $-e_0$, e_0, and 0, respectively. The charge of an atomic nucleus which is composed of protons and neutrons Ze_0 is where Z is

the number of available electrons. Consequently, classical particle dynamics deals with positively and negatively charged atomic and molecular ions, as well as with electrically neutral particles ($e_0 = 0$).

A pair of particles having electric charges e_1 and e_2 can exert either repulsive (if $e_1/e_2 > 0$) or attractive (if $e_1/e_2 < 0$) forces on each other, described by

$$\vec{F}_1 = -\vec{F}_2 = -\vec{\nabla}_i V_C\left(\vec{r}_1, \vec{r}_2\right), \qquad i = 1, 2 \tag{4.62}$$

where $\vec{r}_1$ and $\vec{r}_2$ are radius vectors of the particles and the electrostatic Coulomb potential is

$$V_C\left(\vec{r}_1, \vec{r}_2\right) = V_C\left(r\right) = \frac{1}{4\pi\varepsilon_0}\frac{e_1 e_2}{r}, \qquad r = |\vec{r}_{12}| = |\vec{r}_2 - \vec{r}_1| \tag{4.63}$$

where $\varepsilon_0 = 8.854188 \times 10^{-12}$ C$(V_m)^{-1}$ is the permittivity constant in a vacuum. Equations (4.62) and (4.63) account for the convention where attractive forces are defined as negative sign and repulsive forces are defined as positive sign.

The absolute value of the interaction force in Eq. (4.62) can be shown as a function of the separation distance

$$F_C\left(r\right) = \frac{\partial V\left(r\right)}{\partial r} = \frac{1}{4\pi\varepsilon_0}\frac{e_1 e_2}{r^2} \tag{4.64}$$

For a system of N charged particles, the pair-wise interaction energy is written as

$$U_C = \sum_{i,j>i} V_C\left(r_{ij}\right), \qquad r_{ij} = |\vec{r}_{ij}| = |\vec{r}_j - \vec{r}_i| \tag{4.65}$$

where V_C is the Coulomb potential (4.63) and r_{ij} is the separation distance for a pair of particles i and j. The relevant interaction force can be computed as

$$F_i = -\frac{\partial U}{\partial r_i} = -\left(\frac{\partial}{\partial x_i} + \frac{\partial}{\partial y_i} + \frac{\partial}{\partial z_i}\right) U \equiv -\nabla_i U, \qquad i = 1, 2, \ldots, N \tag{4.66}$$

The Coulomb interaction is noticeable even at large separation distances since the potential (4.63) decays slowly with the growth of r (the separation distance). For this reason, it is called a long-range interaction.

Short-range interaction In the case of a pair of electrically neutral atoms or molecules, the electrostatic field of the positive charges of atomic nuclei or ion is neutralized by the negative charges of electron clouds surrounding the nuclei. In quantum mechanics, the spatial location of electron is described in terms of probability densities in the electron cloud. The term "electron cloud" is in general used in relation to the spatial distributions of these densities. The negative charges of electron clouds experience cross-atomic attraction growing as the distance between the nuclei decreases. At particular distance, which is referred to as the equilibrium (bond) length, this attraction is equilibrated by the repulsive force due to the positive charges of atomic nuclei or ions. The resultant repulsive force increases as the interparticle distance decreases. The potential energy of such a system will be the continuous function of the separation distance if internal quantum states of the electron cloud are not excited.

There exist a number of mathematical models to adequately describe the dual attractive or repulsive character of interactions between a pair of neutral atoms or molecules. The Lennard-Jones potential also called the L-J potential, 6-12 potential or, less commonly, 12-6 potential is a simple mathematical model that

describes this behavior proposed in 1924 by John Lennard-Jones as

$$V_{LJ}(r) = 4\varepsilon\left(\frac{\sigma^{12}}{r^{12}} - \frac{\sigma^{6}}{r^{6}}\right) \tag{4.67}$$

where σ is the characteristic Lennard-Jones length, ε is the characteristic Lennard-Jones energy and r is the interatomic distance.

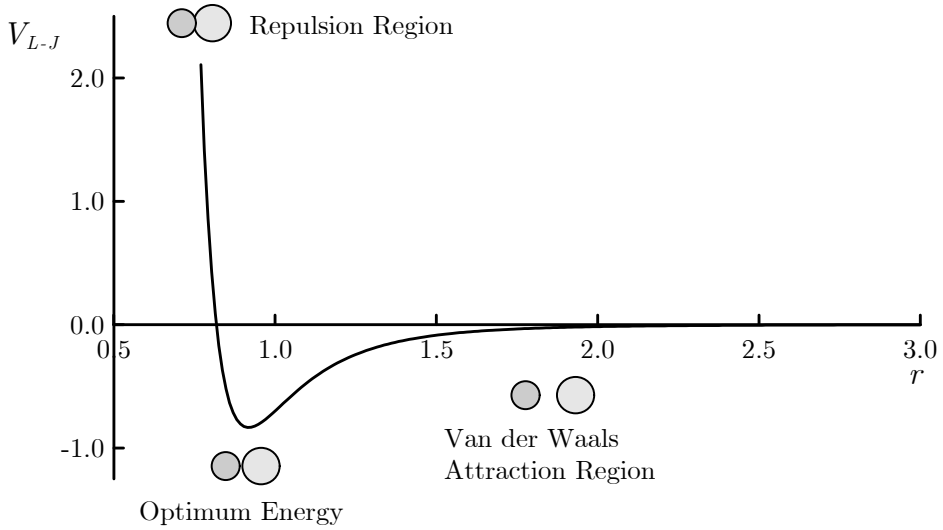

Figure 4.15: The Lennard-Jones potential between a pair of neutral atoms.

Van der Waals attraction occurs at short range and quickly decreases as the interacting atoms move apart by a few Angstroms. Repulsion occurs when the distance between interacting atoms becomes even slightly less than the sum of their contact radii. The $1/r^{12}$ term expresses a strong repulsion based on the Pauli principle. The Pauli principle describes that the electron clouds of atoms are difficult to be overlapped. There exists a strong repulsion and a high energy between electron clouds if they share the orbital boundaries. Therefore, particles tend to move away from each other to minimize the energy. The $1/r^{6}$ term is

based on Van der Waals force giving a weak attraction between atoms with a large distance between them.

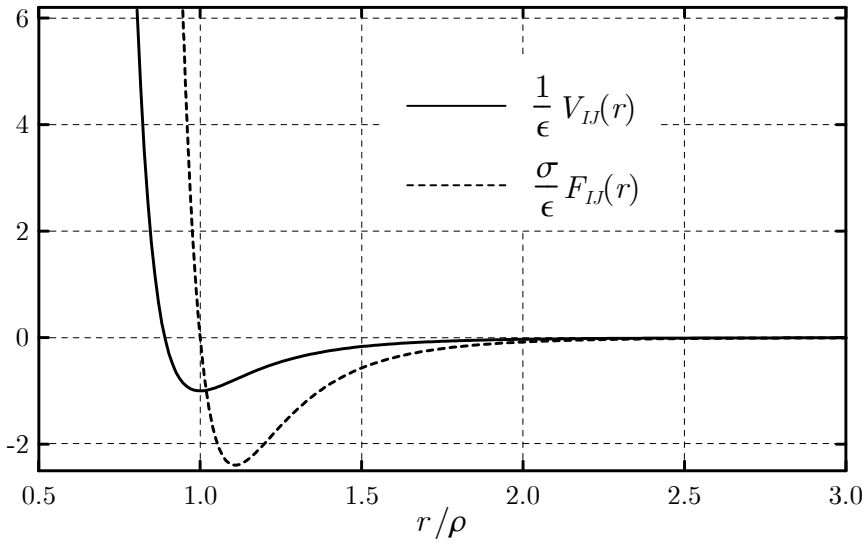

Figure 4.16: Lennard-Jones potential.

The Lennard-Jones (LJ) potential is employed in computer simulations of a great variety of nanoscale systems and processes. Here, σ is the collision diameter, the distance at which $V_{LJ} = 0$ and ε is the dislocation energy. In a typical atomistic system, the collision diameter is equal to several angstroms when 1 Å $= 10^{-10}$ m. The value ε corresponding to the minimum of function in Eq. (4.67), which occurs at the equilibrium bond length $\rho = 2^{1/6}\sigma$ and $V_{LJ}(\rho) = -\varepsilon$. Physically, ε is the amount of work that needs to be done to move the interacting particles apart from the equilibrium distance ρ to infinity. Minimum in the Lennard-Jones potential represents the possibility of bonding for two colliding particles if their relative kinetic energy is less than ε. Since the quantity in brackets is dimensionless, the choice of units for V depends on the definition of ε. Typically, $\varepsilon \approx 10^{-19} \ldots 10^{-18}$

J, so it is more convenient to use a smaller unit rather than joules, such as the electron-volt (eV: 1 eV $= 1.602 \times 10^{-19}$ J). One electron-volt is the work done when an elementary charge like proton is accelerated by an electrostatic field of unit voltage.

The absolute value of the Lennard-Jones interaction force as a function of the interparticle distance is given as

$$F_{LJ}(r) = 24\varepsilon \left(\frac{2\sigma^{12}}{r^{13}} - \frac{\sigma^6}{r^7} \right) \tag{4.68}$$

Another popular model for pair-wise interactions is the Morse potential given by

$$V_M(r) = \varepsilon \left(e^{2\beta(\rho - r)} - 2e^{\beta(\rho - r)} \right) \tag{4.69}$$

and the corresponding force function is

$$F_M(r) = 2\varepsilon\beta \left(e^{2\beta(\rho - r)} - e^{\beta(\rho - r)} \right) \tag{4.70}$$

The Morse potential is usually employed in solid state systems at normal conditions including to elemental metallic systems and alloys. The interaction between neutral particles represented by a Lennard-Jones or a Morse potential is short-range interaction which is contrary to the long-range Coulomb interactions. Short-range potentials are effectively zero if the separation r is larger than several equilibrium separation distances between neutral particles. The Lennard-Jones and Morse potentials are the most common models for short-range pair-wise interactions which are found generally in computational chemistry, physics, and nanoengineering.

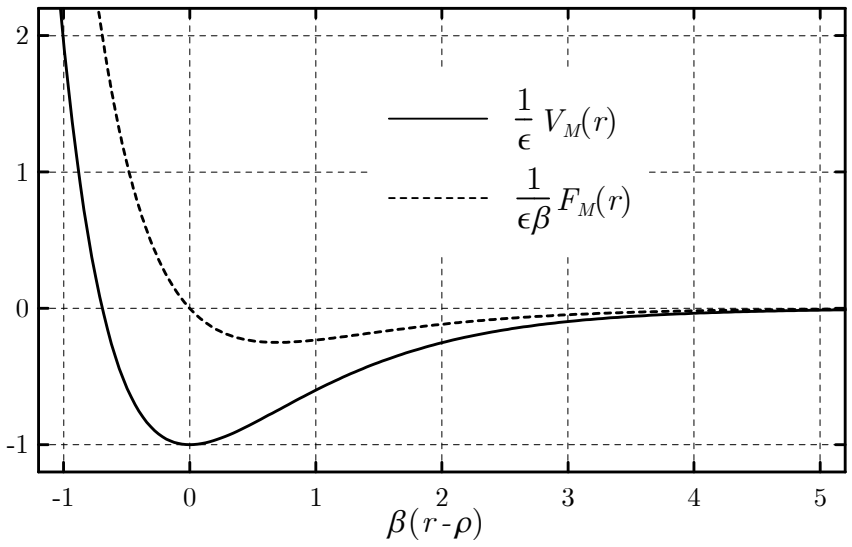

Figure 4.17: Morse potential.

Multibody Interaction The higher-order terms of the potential function is important in complex molecular structures. However, the practical implementation of multibody interactions is complicated, so the multibody effects of the order higher than three are usually neglected. As a result, the three-body potential, V_3, provides contributions to the total potential energy U depending on the value of the angle θ_{ijk} between a pair of interparticle vectors $\vec{r}_{ij}$ and $\vec{r}_{ik}$ formed by three particles i, j, and k.

$$V_3\left(\vec{r}_i, \vec{r}_j, \vec{r}_k\right) = V_3\left(\cos\theta_{ijk}\right), \qquad \cos\theta_{ijk} = \frac{\vec{r}_{ij} \cdot \vec{r}_{ik}}{r_{ij} r_{ik}} \tag{4.71}$$

4.5.3 Microcantilever Deflection due to the Mercury Monolayer Dareing et al. [2] have proposed a model for adsorption-induced surface stress which is based on atomic or molecular interaction. The model is related to the atomic or molecular interactive potential of the adsorbant which is made up of the Lennard-Jones potential and the microcantilever curvature. Total energy of the system is the

sum of this atomic potential in the first layer of atoms attached to a surface of a microcantilever and elastic potential energy in the microcantilever. After total energy is imposed by minimizing the total potential energy, the microcantilever deflection can be determined. Both experimental data and the model were tested with mercury adsorption on gold-coated microcantilevers. The significance of this model is to express the energy potential in the near surface layer of atoms in terms of beam curvature based on the assumptions that adsorbate distribution is uniform over the surface and higher layers of atoms play a minor role to microcantilever's deflection. Also, the experiment was done to check with the simulation model of the microcantilever bending due to adsorption of mercury vapor on the microcantilever surface.

Here, the effects of the surface stress due to mercury adsorption on gold-coated microcantilevers are studied. Based on the numerical data in the literature [2], the results of the surface stress to the microcantilever are investigated by utilizing the three models of surface stress effect as presented above. Forces per atomic width spacing could be determined by minimization of Lennard-Jones potential for moving an atom to the optimum distance.

The dual attractive/repulsive character of interactions between a pair of neutral atoms or molecules can be described as Lennard-Jones potential.

$$V_{LJ}(r) = 4\varepsilon\left(\left(\frac{\sigma}{r}\right)^{12} - \left(\frac{\sigma}{r}\right)^{6}\right) \tag{4.72}$$

In terms of the new constants A and B

$$V_{LJ}(r) = -\frac{A}{r^6} + \frac{B}{r^{12}} \tag{4.73}$$

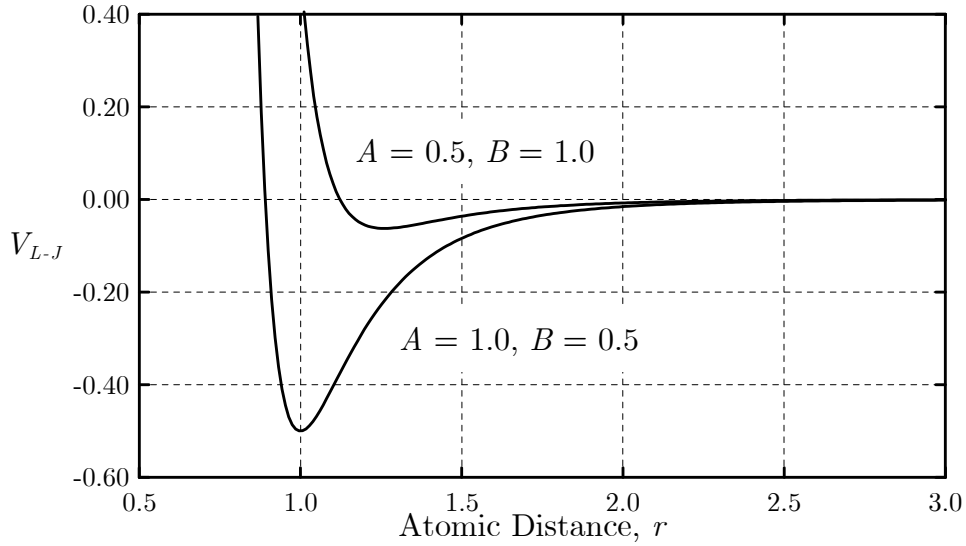

Figure 4.18: The lennard-Jones potential with different parameters A and B.

where $A = 4\varepsilon\sigma^6$ and $B = 4\varepsilon\sigma^{12}$ for which ε is the characteristic Lennard-Jones energy and σ is the characteristic Lennard-Jones length.

The parameter A can be obtained from atomic polarizability measurements or it can be calculated quantum mechanically. The parameter B is basically derived from crystallographic data in order to reproduce observed average contact distances between different kinds of atoms in crystals of various molecules. These two parameters control the depth and interatomic distance of the potential energy well for a pair of non-bonded interacting atoms such as C:C, O:C, O:H, etc. In effect, the parameter A represents the degree of "stickiness" of Van der Waals attraction and B represents the degree of "hardness" of the atoms such as marshmallow-like, billiard ball-like, etc. [69].

The Lennard-Jones potential constants for mercury atoms obtained [70] as $\sigma = 0.2969$ nm and $\varepsilon = 750K \times k$ Joule, where is the Boltzmann constant equal to

1.3805×10^{-23} JK^{-1}. So, these constants can be converted to parameters A and B as

$$A = 2.8377 \times 10^{-77}\ \mathrm{J \cdot m^6} \quad \text{and} \quad B = 1.943 \times 10^{-134}\ \mathrm{J \cdot m^{12}} \tag{4.74}$$

Further input data for the microcantilever are as following: microcantilever length $L = 200\ \mu$m, width $w = 80\ \mu$m, thickness $h_s = 0.7\ \mu$m, material modulus $E = 179$ GPa, atomic spacing of mercury atoms, $b = 0.4$ nm, and the thickness of mercury monolayer, $h_f = 0.45$ nm.

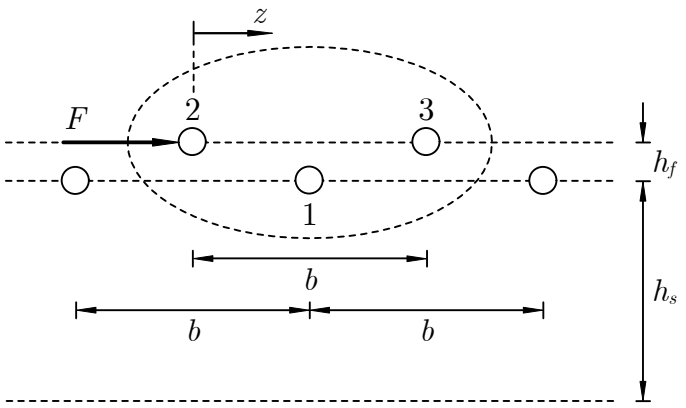

Figure 4.19: Schematic shown relation between force and potential field.

The Lennard-Jones potential between atoms 2 and 3 due to atom 2 moving with distance z is given by

$$U_{2-3}(z) = -\frac{A}{(b-z)^6} + \frac{B}{(b-z)^{12}} \tag{4.75}$$

The potential between atoms 2 and 1 due to atom 2 moving with distance z is

$$U_{2-1}(z) = -\frac{A}{\left(h_f^2 + \left(\frac{b}{2} - z\right)^2\right)^3} + \frac{B}{\left(h_f^2 + \left(\frac{b}{2} - z\right)^2\right)^6} \tag{4.76}$$

Hence, the total potential of moving atom 2 with distance z is

$$U(z) = -\frac{A}{(b-z)^6} + \frac{B}{(b-z)^{12}} - \frac{A}{\left(h_f^2 + \left(\frac{b}{2} - z\right)^2\right)^3} + \frac{B}{\left(h_f^2 + \left(\frac{b}{2} - z\right)^2\right)^6} \quad (4.77)$$

Let F represents the force required to move atom 2 with a distance of dz through the potential field $U(z)$, that is

$$F = \frac{dU(z)}{dz} \quad (4.78)$$

Hence, the force per atomic width spacing b, f, is defined as

$$f = \frac{F}{b} = \frac{1}{b}\frac{dU(z)}{dz} \quad (4.79)$$

Using the material properties of the thin film and geometry parameters of the microcantilever, the force per unit atomic spacing is given by

$$f = -0.190827 \text{ nN/nm} \quad (4.80)$$

This force is then used to obtain the nondimensional surface stress loading paramter βL as

$$\beta L = 1.57686 \quad (4.81)$$

By substituting the loading parameter into the three models for surface stress loading effects, the displacements for the microcantilever are obtained by solving the following sets of differential equations and boundary conditions.

- Stoney's Model (Model I):

$$\frac{d^2\eta}{d\xi^2} = \frac{\alpha}{2}(\beta L)^2 \quad (4.82)$$

$$\eta|_{\xi=0} = 0 \quad \text{and} \quad \left.\frac{d\eta}{d\xi}\right|_{\xi=0} = 0 \quad (4.83)$$

Table 4.4: Tip-deflections of a microcantilever subjected to different models for surface stress effects

Models for Surface Stress Loading Effects	Tip Displacement (nm)
Stoney's Model (Model I)	435
Axial Load Model (Model II)	211
Uniform Surface Force (Model III)	290
Experimental Result [2]	≈ 300

- Axial-Load Model (Model II):

$$\eta'''' - (\beta L)^2 \eta'' = 0 \tag{4.84}$$

$$\eta|_{\xi=0} = 0,\ \eta'|_{\xi=0} = 0,\ \eta''|_{\xi=1} = \frac{\alpha}{2}(\beta L)^2,\ \text{and}\ \eta'''|_{\xi=1} - (\beta L)^2 \eta'|_{\xi=1} = 0 \tag{4.85}$$

- Uniformly Distributed Surface Force (Model III):

$$\eta'''' - \frac{k}{6}\frac{1+\nu}{1-\nu}\alpha^2 (\beta L)^4 \left[(1-\xi)^2 \eta'' - 2(1-\xi)\eta'\right] = 0 \tag{4.86}$$

$$\eta|_{\xi=0} = 0, \quad \eta'|_{\xi=0} = 0, \quad \eta''|_{\xi=1} = 0, \quad \text{and} \quad \eta'''|_{\xi=1} + \frac{\alpha}{2}(\beta L)^2 = 0 \tag{4.87}$$

The corresponding tip deflections of the microcantilever of length $L = 200\ \mu$m for the three models are given in Table 4.8.

Based on the work in [2, 71], Model III gives the best agreement with the experimental result, Model I overestimates while Model II underestimates the experimental tip deflection.

The Microcantilever's Thickness and Its Sensitivity Based on some literature reviews, the microcantilever ranges from 200-300 micrometer length, 20-40 micrometer wide and 0.2-10 micrometer thick. For bio-chemical sensors, it is very important to obtain high sensitivity. A biosensor should detect single proteins and enzymes up to whole cells and microorganisms. The micro size of the cantilever leads to several advantages, such as, high sensitivity, small quantities of substances needed for analysis, and miniaturized sensor devices [24]. Optimization of cantilever dimensions and shapes for maximum stress, temperature or mass sensitivities would be necessary for sensing applications.

In the range of interest here, the atomic force on the microcantilver's surface calculating as force per unit length is approximately 0.2 nN/nm. Therefore, optimization the dimensions in order to detect this small amount of forces is challenging. In this part, forces per unit length and thicknesses have been varied to investigate microcantilever's responses.

The Effects of Lennard Jones Constants to the Bending of a Microcantilever Since microcantilevers are generally used as sensors having high sensitivity to adsorbates that attaches to their surfaces, different attaching substances will effect to bending of the microcantilever differently. Moreover, a pair of neutral atoms can be defined by the attractive (parameter A) and repulsive (parameter B) constants in the Lennard-Jones potential. Therefore, these two parameters would produce the effects to the microcantilever deflections due to atomic adsorption.

As the model of surface stress effects as uniformly distributed forces on the mi-

Table 4.5: Loading parameter for different surface force and beam thicknesses

Surface Force, f	Beam Thickness, h_s (nN/nm)			
(nN/nm)	0.5 μm	1.0 μm	1.5 μm	2.0 μm
-0.05	1.638	0.579	0.315	0.205
-0.10	2.316	0.819	0.446	0.289
-0.15	2.836	1.003	0.546	0.355
-0.20	3.275	1.158	0.630	0.409
-0.25	3.662	1.295	0.705	0.458

Table 4.6: Tip-deflection ($\times 10^{-3}$) by Model I for different beam thicknesses

Surface Force, f	Beam Thickness, h_s (nN/nm)			
(nN/nm)	0.5 μm	1.0 μm	1.5 μm	2.0 μm
-0.05	1.676	0.419	0.186	0.105
-0.10	3.352	0.838	0.372	0.210
-0.15	5.028	1.257	0.548	0.314
-0.20	6.704	1.676	0.745	0.419
-0.25	8.380	2.095	0.931	0.524

Table 4.7: Tip-deflection ($\times 10^{-3}$) by Model II for different beam thicknesses

Surface Force, f	Beam Thickness, h_s (nN/nm)			
(nN/nm)	0.5 μm	1.0 μm	1.5 μm	2.0 μm
-0.05	0.781	0.368	0.179	0.103
-0.10	1.006	0.654	0.344	0.202
-0.15	1.104	0.883	0.497	0.299
-0.20	1.156	1.070	0.639	0.392
-0.25	1.186	1.226	0.771	0.482

Table 4.8: Tip-deflection ($\times 10^{-3}$) by Model III for different beam thicknesses

Surface Force, f	Beam Thickness, h_s (nN/nm)			
(nN/nm)	0.5 μm	1.0 μm	1.5 μm	2.0 μm
-0.05	1.117	0.279	0.124	0.070
-0.10	2.235	0.559	0.248	0.140
-0.15	3.352	0.838	0.372	0.210
-0.20	4.469	1.117	0.496	0.279
-0.25	5.587	1.397	0.621	0.349

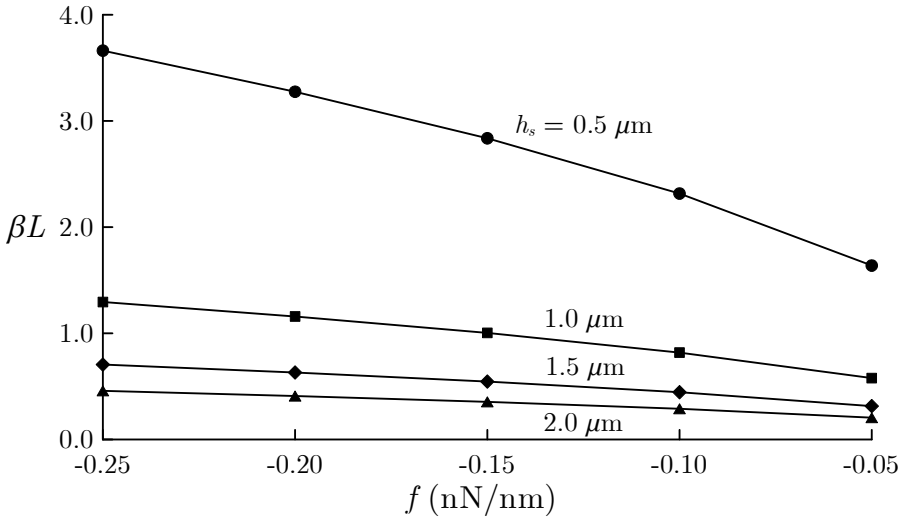

Figure 4.20: Loading parameter βL vs. surface force f for various beam thicknesses, h_s.

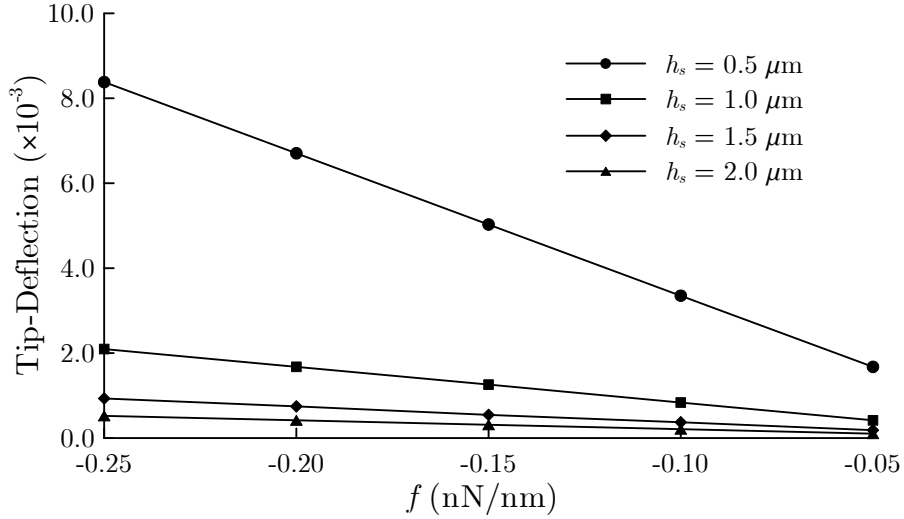

Figure 4.21: Tip-deflection vs. surface force by Model I for various beam thicknesses.

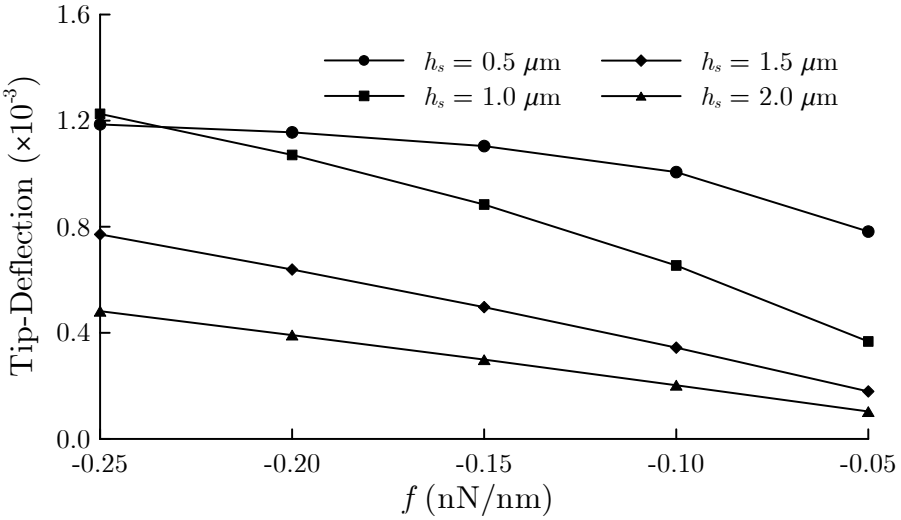

Figure 4.22: Tip-deflection vs. surface force by Model II for various beam thicknesses.

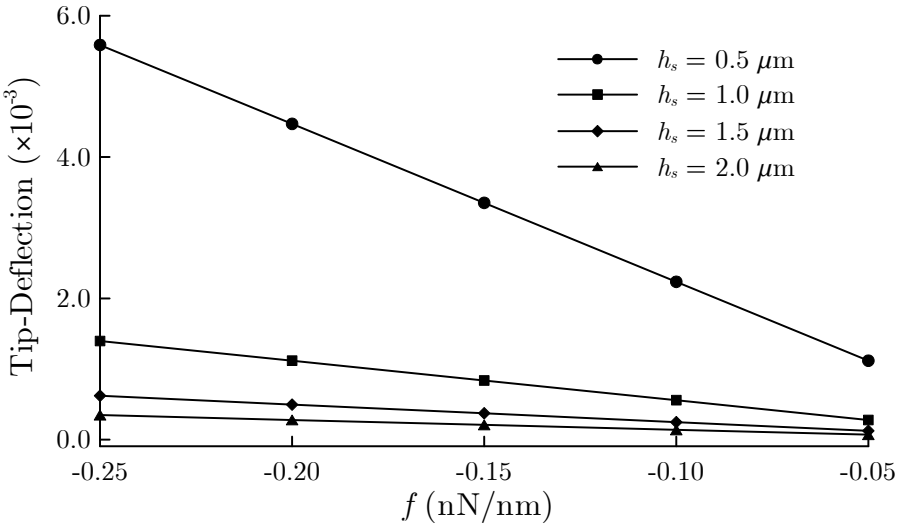

Figure 4.23: Tip-deflection vs. surface force by Model III for various beam thicknesses.

Table 4.9: Tip-deflections of a microcantilever for different values of Lennard-Jones constants

A	B	Atomic Force	Tip-Deflection
$(\mathrm{J}\cdot\mathrm{m}^6\times10^{-77})$	$(\mathrm{J}\cdot\mathrm{m}^{12}\times10^{-134})$	(nN/nm)	$(\times10^{-3})$
1	1	-0.04215	0.320
2	1	-0.18475	3.939
1	2	-0.00440	0.033
1	3	0.07731	-0.588

crocantilever surface compares favorably with the experimental result, this model will be employed to study the effects of Lennard-Jones constants and atomic spacing plus thickness of atomic monolayer of the coating. Similar to the method as shown above, deflections of the microcantilever with atomic spacing of 0.40 nm and atomic monolayer of 0.45 nm can be determined.

From Table 4.9, it could be concluded that the deflection increases when A increases. Since A represents attractive forces that tend to move atoms closer together. The higher A is, the more the deflection will be. But if B increases, atoms will repel each other when B reaches a certain value, the microcantilever would have a negative curvature.

The Effects of the Monolayer's Thickness and Atomic Spacing of Mercury Atoms to the Deflections Based on the method to find forces per unit atomic width of a

Table 4.10: Surface stress loading parameters with different values of layer thickness and atomic spacing

Atomic Spacing, b	Monolayer Thickness, h_f (nm)		
(nm)	0.40	0.45	0.50
0.40	1.654	1.577	1.537
0.45	1.503	1.423	1.381
0.50	1.329	1.248	1.205

mercury monolayer coating as shown above and the model of surface stress effect due to uniformly distributed forces on the microcantilever surface, the effects of the monolayer's thickness and atomic spacing of mercury atoms to the deflections are investigated.

The input data for the microcantilever are as following: microcantilever length $L = 200$ μm, width $w = 80$ μm, thickness $h_s = 0.7$ μm, material modulus $E = 179$ GPa. For mercury atoms, $A = 2.8377 \times 10^{-77}$ J·m^6 and $B = 1.9430 \times 10^{-134}$ J·m^{12}, the microcantilever deflection can be calculated. Variations of surface stress loading parameter, βL, with layer thickness, h_f, and atomic spacing, b, are shown in Table 4.10.

The Table below shows dimensionless microcantilever tip-deflections with varied the atomic spacing, b, and thickness of a monolayer h_f.

Table 4.11: Tip-deflection with different values of layer thickness and atomic spacing

Atomic Spacing, b	Monolayer Thickness, h_f (nm)		
(nm)	0.40	0.45	0.50
0.40	1.528×10^{-3}	1.450×10^{-3}	1.379×10^{-3}
0.45	1.318×10^{-3}	1.181×10^{-3}	1.113×10^{-3}
0.50	1.030×10^{-3}	0.908×10^{-3}	0.848×10^{-3}

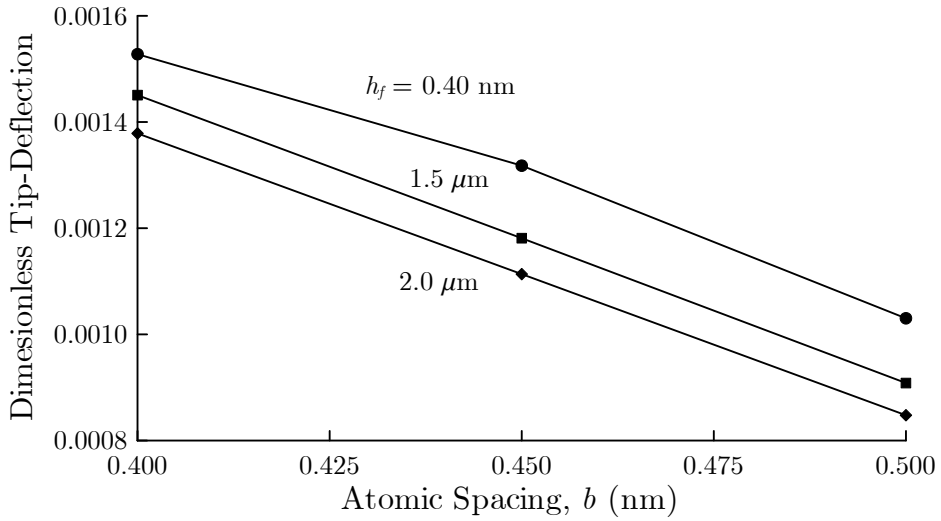

Figure 4.24: Influence of atomic spacing and thickness of atomic monolayer on the tip deflection of a microcantilever.

CHAPTER 5

Results and Discussions

The recent availability of silicon microfabrication and surface functionalization techniques offer the possibilities of developing microscopic devices that possess unique characteristics such as micromechanical transducer for biological and chemical detection. A micromechanical cantilever, commonly fabricated from Si, SiN, or polymers and is similar to a probe used in Atomic Force Microscope (AFM), is generally found in the field of Microelectromechanical Systems (MEMS) and Nanoelectromechanical Systems (NEMS). Microcantilever is widely employed in the field of sensors due to its two favorable operational modes- resonant frequency variation due to mass loading and bending deformation due to atomic or molecular adsorption that creates uneven surface stress loading. It acts as a transducer that transforms load effects into measurable mechanical responses with high sensitivity. In the present work, research is focused on the mechanical response of a microcantilever subjected to surface stress loading that arises from atomic or molecular adsorption on one of its surface. The molecular absorption and interfacial chemical reactions may produce satisfactory deformation of the microcantilever that can be effectively used for micro/nano sensing applications.

The sources of the surface stress can be described as atomistic interactions between surface atoms, intermolecular forces between absorbed molecules, temperature changes, and phase transitions. From an atomistic viewpoint, surface

stress is formed by non-uniform charge distribution such that the one for the bulk material and the one for the material near the surface are different. When there is an absence of atoms above the free surface, electrons and electronic charges will rearrange themselves. This causes net unbalanced forces acting on the atoms that are in the vicinity of the surface. If this effect results in unequal stresses on the opposite sides of a beam or thin plate, the structure will bend with a radius of curvature. The surface stress and substrate curvature are generally described by Stoney formula which assumed small deflection with a uniform curvature. Due to the simplified assumptions introduced in the formulation, it always overestimates the deflections.

Three models for the effects of surface stress on a micromechanical cantilever are investigated. The first model (Model I) is based on the Stoney's formulation that describes the effects of surface stress loading to the beam as a concentrated moment applied at the free-end of the microcantilever. Next model (Model II) is also based on the Stoney's formulation, but it takes into account the effect of an additional axial force applied at the free-end of the beam. In the third model (Model III), the effects of surface stress loading are considered as a uniformly distributed force per unit length acting on the upper surface of the microcantilever. As a result, this surface loading causes load effects on the beam in terms of a uniformly distributed bending moment and uniformly distributed axial force applied along the microcantilever axis. In the first two models, the effects of surface stress on the displacement of the microcantilever are calculated by introducing the

Euler-Bernoulli beam theory, which is generally employed to analyze beams with small deflection. In the third model, the energy method is employed to derive the governing equation for beam deflection together with a set of proper boundary conditions. The numerical methods, such as the finite element method can then be introduced to obtain the solution.

A microcantilever with thickness to length ratio $\alpha = 0.05$ is considered in this study. The deflections of the microcantilever are then calculated subjected to different loading conditions described by the effects of surface stress models. The results of Models I and II are comparable when subjected to small amplitude surface stress loading. Model III gives the smallest deflection comparing with the first two models. This is due to the fact that when the effect of surface stress is modeled as a concentrated moment applied at the free-end (Models I and II), it maximizes the bending deformation of the beam. For Model III, the bending moment is uniformly distributed along the beam. For high amplitude surface stress loading, the results predicted by Model II are clearly smaller than that by Model I. This is caused by stiffening effect of the resultant tensile force applied at the free-end of the microcantilever in Model II. Whereas Model III predicted larger deflections than that of Model II, because uniformly distributed tensile axial force applied on the surface and concentrated tensile axial loads applied at the free-end result in different stiffening effects. The tensile concentrated axial force applied at the free-end of the cantilever provides a larger stiffening effect and, as a result, gives in smaller deflections.

Generally, the origins of surface stress are described as a result of molecular or atomic adsorption on the microcantilever. In the present work, a monolayer of mercury as the atomic adsorption on the microcantilever is studied; the Lennard-Jones potential is then employed to describe the dual attractive or repulsive interactions between a pair of mercury atoms. Force per unit length of a mercury monolayer is calculated by the input data of the Lennard-Jones constants, atomic spacing of the atoms, and thickness of the monolayer. Based on the three models of surface stress effects, these forces induced in the surface atoms is substituted in the governing equations for the three models. The deflection results are compared with the experimental data in published literature. As expected, the result of Model I show to overestimate deflection, Model II gives the underestimated deflection, and Model III shows the most favorable results.

Since the result of Model III agreed well with the experiment, it is introduced to further study the effects of the Lennard-Jones constants, atomic spacing, and monolayer thickness to the microcantilever deflection. The physical property of the adsorbates can be defined by the attractive, A, and repulsive, B, parameters of the Lennard-Jones potential. These two parameters define the characteristics of the surface stress and, in turn, directly affect the displacement response of the microcantilever. Microcantilever deflections with atomic spacing of 0.4 nm and atomic monolayer of 0.45 nm can then be determined with varied Lennard-Jones constants. The result has shown that the deflections increase when A increases, since A represents the attractive forces that tend to move atoms closer together.

The larger the value of A, the beam experiences more upward deflection. If the value of B increases, atoms will repel each other and when B reaches a certain value, the microcantilever will have a negative curvature. Since the atomic spacing between mercury atoms is approximately 0.4 nm, here the spacing and monolayer thickness are then varied between the range of 0.4 -0.5 nm. The largest deflection is found to occur at the smallest values of the atomic spacing (0.4 nm) and monolayer thickness (0.4 nm). This is because the Lennard-Jones potential is the short-range interaction; it gives a larger interatomic force for a minimum value of spacing. Also thin film has larger film stress than thick film, so it induces a larger force onto the substrate, thus leads to a larger deflection.

Proposed models take into account the intermolecular interaction force between the adsorbed atoms and the substrate atoms. The model gives insight into the interatomic forces which play a significant role in creating adsorption-induced surface stress and resulting bending deformation of a microcantilever. With some refinements, Model III which modeled the surface stress as a uniformly distributed force per unit length on the surface can used to predict the deflection of a microcantilever sensor under more complex molecular adsorption problems.

5.1 Future Works

- Experimental work needs to be conducted to better understand the surface stress effects.

- With some refinement and more understanding in mechanics of surface atoms, the stress models can be employed to predict the microcantilever deflections

due to more complex molecular adsorption.

- Introducing other potentials for interactions between surface atoms.

- Since scaling-down of the macro devices might increase the nonlinearity, nonlinear analysis of microcantilevers under surface stress loading conditions should be conducted.

- As the static mode of a microcantilever in sensing applications has a weak point that the material properties like Young's modulus is needed, this would make a significant error in the calculation. Then the vibration mode should be performed.

- Develop the optimization of cantilever dimensions and shapes for higher sensitivity and the using of the arrays of cantilevers in parallel.

- Deflections due to different shapes of microcantilevers should be investigated such as V-shape.

REFERENCES

[1] Ventra, M. D., Evoy, S. and Heflin, J. R., 2004, *Introduction to Nanoscale Science and Technology*, Springer Science+Business Media, Inc., USA.

[2] Dareing, D.W. and Thundat, T. 2005, "Simulation of Adsorption-induced Stress of a Micromicrocantilever Sensor," *J. Appl. Phys.* **97**, pp. 043526.

[3] Zhang, Y., Ren, Q. and Zhao, Y., 2004, "Modelling Analysis of Surface Stress on a Rectangular Microcantilever Beam," *J. Phys. D: Appl. Phys.* **37**, pp. 2140-2145.

[4] Feynman, R. P., 1992, "There's Plenty of Room at the Bottom," *J. Micro. Sys.*, **1**, pp. 60-66.

[5] Feynman, R. P., 1993, "Infinitesimal Machinery," *J. Micro. Sys.*, **2**, pp. 4-14.

[6] Binnig, G. and Rohrer, H., 1987, "Scanning Tunneling Microscopy-from Birth to Adolescence," *Rev. Mod. Phys.*, **59**, pp. 615-625.

[7] Binnig, G. and Quate, C.F., 1986, "Atomic Force Microscope," *Phys. Rev. Lett.*, **9**, pp. 930-934.

[8] Viani, M. B., 1999, "Small Cantilevers for Force Spectroscopy of Single Molecules," *J. Appl. Phys.*, **86**, pp. 2258-2262.

[9] AZoM.com Pty Ltd., "A Review of Microcantilevers for Sensing Applications", http://www.azonano.com/Details.asp?ArticleID=1927.

[10] Evans, D. R. and Craig, V. S., 2006, "Sensing Cantilever Beam Bending by the Optical Lever Technique and Its Application to Surface Stress," *J. Phys. Chem. B*, **110**, pp. 5450- 5461.

[11] Barnes, J. R., Stephenson, R. J., Welland, M. E., Gerber, Ch., and Gimzewski, J. K., 1994, "Photothermal Spectroscopy with Femtojoule Sensitivity using a Micromechanical Device," *Nature*, **372**, pp. 79-81.

[12] Oden, P. I., Chen, G. Y., Steele, R. A., Warmack, R. J., and Thundat, T., "Viscous Drag Measurements Utilizing Microfabricated Cantilevers," *Appl. Phys. Lett.*, **68**, pp. 3814-3816.

[13] Ilic, B., Czaplewski, D., Zalalutdinov, M., Craighead, H. G., Neuzil, P., Campagnolo, C., and Batt., C., 2001, "Single Cell Detection with Micromechanical Oscillators," *J. Vac. Sci. Technol. B*, **19**, pp. 2825-2828.

[14] Thundat, T., Warmack, R. J., Chen, G.Y., and Allison, D. P., 1994, "Thermal and Ambient-Induced Deflections of Scanning Force Microscope Cantilevers," *Appl. Phys. Lett.*, **64**, pp. 2894-2896.

[15] Chen, G. Y., Thundat, T., Wachter, E. A. and Warmack, 1995, R. J., "Adsorption-Induced Surface Stress and Its Effects on Resonance of Frequency of Microcantilevers," *J. Appl. Phys.*, **77**, pp. 3618-3622.

[16] Berger, R., Delamarche, E., Lang, H. P., Gerber, C., Gimzewski, J. K., Meyer, E., and Guntherodt, H. J., 1997, "Surface Stress in the Self-Assembled of Alkanethiols on Gold," , *Science*, **276**, pp. 2021-2024.

[17] Wu, G., Ji, H., Thundat, T., Datar, R., Cote, R., Hagan, M. F., Chakraborty, A. K., and Majumdar, A., 2001, "Origin of Nanomechanical Cantilever Motion Generated from Biomolecular Interactions," *PNAS*, **98**, pp. 1560-1564.

[18] Fritz, J. et al., 2000, "Translating Biomolecular Recognition into Nanomechanics," *Science*, **288**, pp. 316-318.

[19] Godin, M., Williams, P. J., Tabard-cossa, V., Laroche, O., Beaulieu, L. Y., Lennox, R. B., and Grutter, P., 2004, "Surface Stress, Kinetics, and Structure of Alkanethiol Self-Assembled Monolayers," *Langmuir*, **20**, pp. 7090-7096.

[20] Luo, C., 2005, "Inaccuracy in the Detection of Molecules Using Two Microcantilever-Based Methods," **72**, pp. 617-619.

[21] Hwang, K. S., Eom, K., Lee, J. H., Chun, D. W., Cha, B. H., Yoon, D. S., and Kim, T. S., 2006, "Dominant Surface Stress Driven by Biomolecular Interactions in the Dynamical Response of Nanomechanical Microcantilevers," *Appl. Phys. Lett.*, **89**, pp. 173905-3.

[22] Gittes, F. and Schmidt, C. F., 1998, "Thermal Noise Limitations on Micromechanical Experiments," *Eur. Biophys. J.*, **27**, pp. 75-81.

[23] Sander, D., 2003, "Surface Stress: Implications and Measurements," Curr. Opin. Solid St. M., **7**, pp. 51-57.

[24] Raiteri, R., Butt, H. J. and Grattarola, M., 1998, "Changes in Surface Stress Measured with an Atomic Force Microscope," *Scanning Microsc.*, **12**, pp. 243-251.

[25] Ibach, H., 1997, "The Role Surface Stress in Reconstruction, Epitaxial Growth and Stabilization of Mesoscopic Structures," *Surf. Sci. Rep.*, **29**, pp. 193-263.

[26] Schell-Sorokin, A. J., and Tromp, R. M., 1990, "Mechanical Stresses in (sub) Monolayer Epitaxial Films," *Phys. Rev. Lett.*, **64**, pp. 1039-1042.

[27] Haiss, W., 1996, "Quantitative Surface Stress Measurements on Au (111) Electrodes by Scanning Tunneling Microscopy," *Langmuir*, **12**, pp. 4311-4313.

[28] Leiva, E. P. M., Del Popolo, M. G. and Schmickler, W., 2000, "Changes in Surface Stress Caused by the Adsorption of an Epitaxial Metal Monolayer," *Chem. Phys. Lett.*, **320**, pp. 392-397.

[29] Fritz, J., Baller, M. K., Lang, H. P., Strunz, T., Meyer, T., Guntherodt, H. J., Delamarche, E., Gerber, Ch., and Gimzewski, J. K., 2000, "Stress at the Solid-Liquid Interface of Self-Assembled Monolayers on Gold Investigated with Nanomechanical Sensor," *Langmuir*, **16**, pp. 9694-9696.

[30] Ibach, H., 1999, "Erratum to: The Role of Surface Stress in Reconstruction, Epitaxial Growth and Stabilization of Mesoscopic Structures," *Surf. Sci. Rep.*, **35**, pp. 71-73.

[31] Dahmen, K., Lehwald, S., and Ibach, H., 2000, "Bending of Crystalline Plates under the Influence of Surface Stress-a Finite Element Analysis," *Surf. Sci.*, **446**, pp. 161-173.

[32] Stoney, G. G., 1909, "The Tension of Metallic Films Deposited by Electrolysis," *Proc. R. Soc. Lond. Ser. A*, **82**, pp. 172-175.

[33] Freund, L. B., Floro, J. A., Chason, E., 1999, "Extension of the Stoney Formula for Substrate Curvature to Configurations with Thin Substrates or Large Deformations," *Appl. Phys. Lett.*, **74**, pp. 1987-1989.

[34] Klein, C. A., 2000, "How Accurate Are Stoney's Equation and Recent Modifications," *J. Appl. Phys.*, **89**, pp. 5487-5489.

[35] Ngo, D., Huang, Y., Rosakis, A. J. and Feng, X., 2006, "Spatially Non-Uniform, Isotropic Misfit Strain in Thin Films Bonded on Plate Substrates: The Relation between Non-Uniform Film Stresses and System Curvatures," Thin Solid Films, **515**, pp. 2220-2229.

[36] Feng, X., Huang, Y., Jiang, H., Ngo, D., and Rosakis, A. J., 2006, "The Effect of Thin Film/Substrate Radii on the Stoney Formula for Thin Film/Substrate Subjected to Nonuniform Axisymmetric Misfit Strain and Temperature," *J. Mech. Mater. Struct.*, **6**, pp. 1041-1053.

[37] Sader, J. E., "Surface Stress Induced Deflections of Cantilever Plates with Applications to the Atomic Force Microscope: Rectangular Plates," *J. Appl. Phys.*, **89**, pp. 2911-2921.

[38] Godin, M., Tabard-Cossa, V., Grutter, P. and Williams, P., 2001, "Quantitative Surface Stress Measurements Using a Microcantilever," *Appl. Phys. Lett.*, **79**, pp. 551-553.

[39] Miyatani, T., and Fujihira, M., 1997, "Calibration of Surface Stress Measurements with Atomic Force Microscopy," *J. Appl. Phys.*, **81**, pp. 7099-7115.

[40] Ramos, D., Mertens, J., Calleja, M., and Tamayo, J., 2007, "Study of the Origin of Bending Induced by Bimetallic Effect on Microcantilever," *Sensors*, **7**, pp. 1757-1759.

[41] McFarland, A. W., Poggi, M. A., Doyle, M. J. and Bottomley, L. A., 2005, "Influence of Surface Stress on the Resonance Behavior of Microcantilevers," *Appl. Phys. Lett.*, **87**, pp. 053505.

[42] Liu, F., Rugheimer, P., Mateeva, E., Savage, D. E., Legally, M. G., 2002, "Response of a Strained Semiconductor Structure," *Nature*, **416**, pp. 498.

[43] Changizi, M. A., 2006, "Nonlinear versus Linear Deflection Analysis of Microcantilever," *IEEE, ISIE*, pp. 3322-3327.

[44] Freund, L. B., and Suresh, S., 2004, *Thin Film Materials; Defect Formation and Surface Evolution*, Cambridge University Press, Cambridge, UK.

[45] Doerner, M. F. and Nix, W. D., 1986, "Stresses and Deformation Processes in Thin Films on Substrate," *CRC Critical Reviews in Solid State and Materials Sciences*, **14**, pp. 225-268.

[46] Landau, L. D. and Lifshitz, E. M., 1986, *Theory of Elasticity*, New York, Pergamon Press.

[47] Schwarzer, N. and Richter, F., "On the Determination of Film Stress from Substrate Bending: Stoney's Formula and Its Limits," http://archiv.tu-chemnitz.de/pub/2006/0011/index.html.

[48] Godin, M., *Surface Stress, Kinetics, and Structure of Alkanethiol Self-Assembled Monolayers*, Ph. D. Dissertation, McGill University, 2004.

[49] Ibach, H., 1994, "Adsorbate-Induced Surface stress," *J. Vac. Sci. Techno. A*, **4**, pp. 2240-2245.

[50] Shuttleworth, R., 1950, "The Surface Tension of Solids," *Proc. Phys. Soc., London, Sect. A.*, **63**, pp. 444-457.

[51] Raiteri, R., Grattarola, M., Butt, H. and Skladal, P., 2001, "Micromechanical Cantilever-based Biosensors," *Sensors and Actuators B*, **79**, pp. 115-126.

[52] Wu, G. H., Datar, R. H., Hansen, K. M., Thundat, T., Cote, R. J., and Majumdar, A., 2001, "Bioassay of Prostate-Specific Antigen (PSA) Using Microcantilever," *Nat. Biotechnol.*, **19**, pp. 856-860.

[53] Baselt, D. R., et al., 2003, "Design and Performance of a Microcantilever-Based Hydrogen Sensor," *Sensors and Actuators B*, **88**, pp. 120-131.

[54] Gimzewski, J. K., Gerber, Ch., Meyer, E. and Schlittler, R. R., 1994, "Observation of a Chemical Reaction Using a Micromechanical Sensor," *Chemical Physics Letters*, pp. 589-594.

[55] Gupta, A., Akin, D., and Bashir, R., 2004, "Single Virus Particle Mass Detection Using Microresonators with Nanoscale Thickness," *Appl. Phys. Lett.*, **84**, pp. 1976-1978.

[56] Ilic, B. et al., 2004, "Attomgram Detection Using Nanoelectromechanical Oscillators," *J. Appl. Phys.*, **95**, pp. 3694-3703.

[57] Lang, H. P. et al., 1999, "An Artificial Nose Based on Micromechanical Cantilever Array," *Analytica Chimica Acta*, **393**, pp. 59-65.

[58] Ji, H. F., Thundat, T., Dabestani, R., Brown, G. M., Britt, P. F., and Bonnesen, P. V., 2001, "Ultrasensitive Detection of CrO42- Using a Microcantilever Sensor," *Anal. Chem.*, **73**, pp. 1572-1576.

[59] Lang, H. P., Hegner, M., Meyer, E., and Gerber, Ch., 2002, "Nanomechanics from Atomic Resolution to Molecular Recognition Based on Atomic Force Microscopy Technology," *Nanotechnology*, **13**, pp. R29-R36.

[60] Erlandsson, R., McClelland, G. M., Mate, C. M. and Chiang, S., 1987, "Atomic Force Microscopy Using Optical Interferometry," *J. Vac. Sci. Technol.*, **6**, pp. 266-270.

[61] Tortonese, M., Barrett, R. C. and Quate, C. F., 1993, "Atomic Resolution with An Atomic Force Microscope Using Piezoresistive Detection," *Appl. Phys. Lett.*, **62**, pp. 834-836.

[62] Ugural, A. C., Fenster, S. K., *Advanced Strength and Applied Elasticity*, Pearson Education, Inc., New Jersey, USA.

[63] Langhaar, Henry L., 1962, *Energy Methods in Applied Mechanics*, John Wiley & Sons, Inc., USA.

[64] Pelesko, J. A. and Bernstein, D. H., 2003, *Modeling MEMS and NEMS*, Chapman & Hall/CRC, USA.

[65] http://www.memsnet.org /material/siliconsibulk

[66] Reddy, J. N., 2005, *An Introduction to the Finite Element Method*, McGraw-Hill, New York, USA.

[67] Pepper, D. W. and Henrich, J. C., 2006, *The Finite Element Method: Basic Concepts and Applications*, Taylor & Francis, New York, USA.

[68] Liu, W. K., Karpov, E. G. and Park, H. S., 2006, *Nano Mechanics and Materials: Theory, Multiscale Methods and Applications*, John Wiley & Sons, New York.

[69] http://cmm.cit.nih.gov/modeling/guide_documents/molecular_mechanics_document.html.

[70] Reid, R. C., Prausnitz, J. M. and Poling, B. E., 1987, *The Properties of Gases and Liquids*, 4th ed., McGraw-Hill, New York, USA.

[71] Miyatani, T. and Fujihira, M., 1997, "Calibration of Surface Stress Measurements with Atomic Force Microscopy," *J. Appl. Phys.* **81**, pp. 7099-7115.